AD-A118 765 NAVAL OCEAN RESEARCH AND DEVELOPMENT ACTIVITY NSTL S--ETC F/G 8/10
SOUND SPEED STRUCTURE OF THE WESTERN SOUTH ATLANTIC OCEAN.(U)
JUL 82 D F FENNER

UNCLASSIFIED NORDA-TN-107 NL

END
DATE FILMED
9-82
DTIC

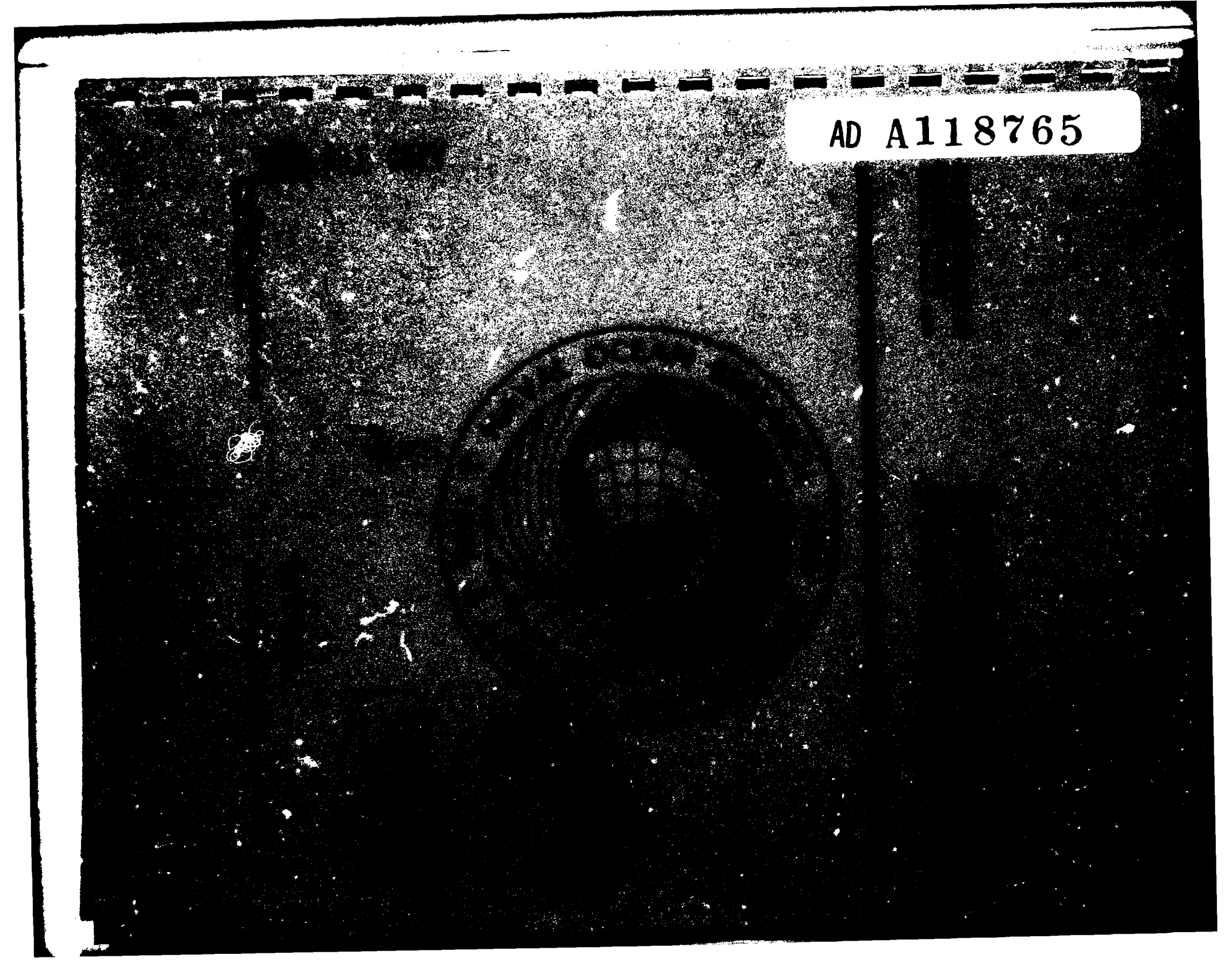

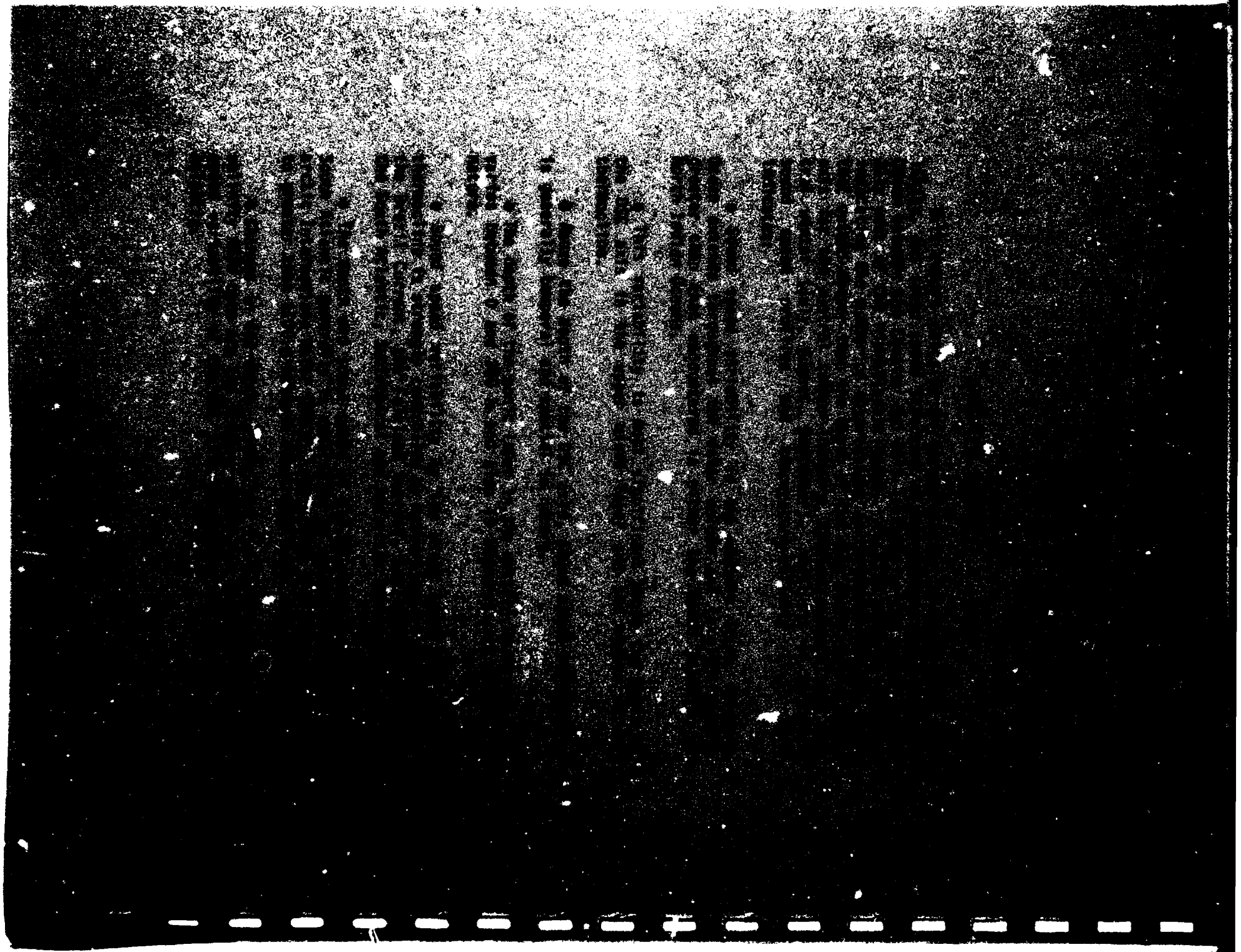

- Changes in depth, width, and T-S structure of the Mediterranean Intermediate Water (MIW) high salinity core causes higher sound speed values at depths between 1750 m and 2500 m and frequently causes the formation of sound speed perturbations throughout the western South Atlantic.

- Below about 3000 m depth, sound speed variability throughout the western South Atlantic is substantially greater than that encountered in the North Atlantic Ocean.

- This variability is caused by northward flowing, low salinity, near-bottom Antarctic Bottom Water (AABW) and mixing between the bottom of the MIW layer and the top of the AABW layer.

- AABW lowers near-bottom sound speed values and changes near-bottom sound speed gradients throughout the western South Atlantic Ocean.

- The great sound speed variability encountered throughout the western South Atlantic Ocean undoubtedly has pronounced effects on sound propagation throughout the study area.

ACKNOWLEDGMENTS

The author wishes to thank the people who made this technical note possible, and there are many involved. First of all, special thanks must be given to Louis P. Solomon, Robert F. Gardner, and Jones Hicks Ford for the inspiration, patience and understanding. Second, special thanks are given to Margaret Chrissinger for continuous typing. Third, the long, hard job of drafting must be credited to both Joanne Lackie and Maryellen Turcotte. Finally, thanks are extended to Linda McRaney for final editing. Thank you all, very, very much.

CONTENTS

TABLES

ILLUSTRATIONS.

SONAR SPEED STRUCTURE OF THE WESTERN SOUTH ATLANTIC OCEAN

I. INTRODUCTION

The sound speed structure of the South Atlantic Ocean is entirely different from that of the North Atlantic Ocean. This difference is due to a different circulation pattern south of the Equator and the hemispheric position of the south Atlantic Ocean. In the south Atlantic, austral summer is defined as January through March, and austral winter is defined as July through September. Figure 1 shows the Marsden Square system for the South Atlantic between the Equator and 60° latitude. However, in this report, only the region north of 45°S to 50°S latitude and west of the Mid-Atlantic Ridge will be discussed in terms of sound speed structure. All sound speed profiles presented have been calculated using the equation of Mackenzie (1981) rather than the equation of Wilson (1960), the former being a more accurate equation in the opinion of the author.

II. SOUTH ATLANTIC CIRCULATION

The general circulation pattern of the South Atlantic Ocean in relation to underwater sound speed has been reported previously by Fenner (1981) and Feuillet (1981). Figure 2 shows the surface circulation pattern of the South Atlantic after Miller (1966). Frontal positions on Figure 2 are from Defant (1961) but are largely based on works by Wust (1936). In the South Atlantic, cold water circulation is generally more pronounced than that found in the North Atlantic or North Indian Oceans. The most important cold water circulation in the South Atlantic is the West Wind Drift (part of the Antarctic Circumpolar Current). This cold water circulation is separated from the remainder of the South Atlantic by the Antarctic Convergence.

The Benguela Current transports large amounts of cold Antarctic water into the eastern South Atlantic off the west coast of Africa. As the Benguela Current flows northward, it warms, undergoes the influence of Coriolis force and, at about 15°S latitude, turns to the west to form the South Equatorial Current. This warm water current flows across the Equatorial Atlantic to about 30°W longitude. At 30°W, the South Equatorial Current splits into two parts. The northern part of the South Equatorial Current crosses the Equator and enters the North Atlantic Ocean. The southern part of the South Equatorial Current turns southward to form the Brazil Current. The Brazil Current flows southward in the western South Atlantic to about 40°S latitude where it meets the cold, northward flowing Falkland Current in the vicinity of the South Atlantic Subtropical Convergence. The Falkland Current has no counterpart in any other ocean and, according to Miller (1966), is either caused by prevailing winds or the projection of the tip of South America into the West Wind Drift.

Although the counterclockwise circulation pattern of the South Atlantic Ocean is moderately well developed, extremely large amounts of cold Antarctic water are carried into the South Atlantic by both the Benguela and Falkland Currents. Other than the South Equatorial Current and Brazil Current, the only other warm water currents found in the South Atlantic are the Guinea Current north of 10°S latitude and the Agulhas Current south of the Cape of Good Hope. More importantly, the extreme intermixing between warm and cold water currents that occurs off the east coast of South America and south of the Cape of Good Hope causes the formation of regions of mesoscale oceanographic variability. Such variability could have significant effects on sound speed structures.

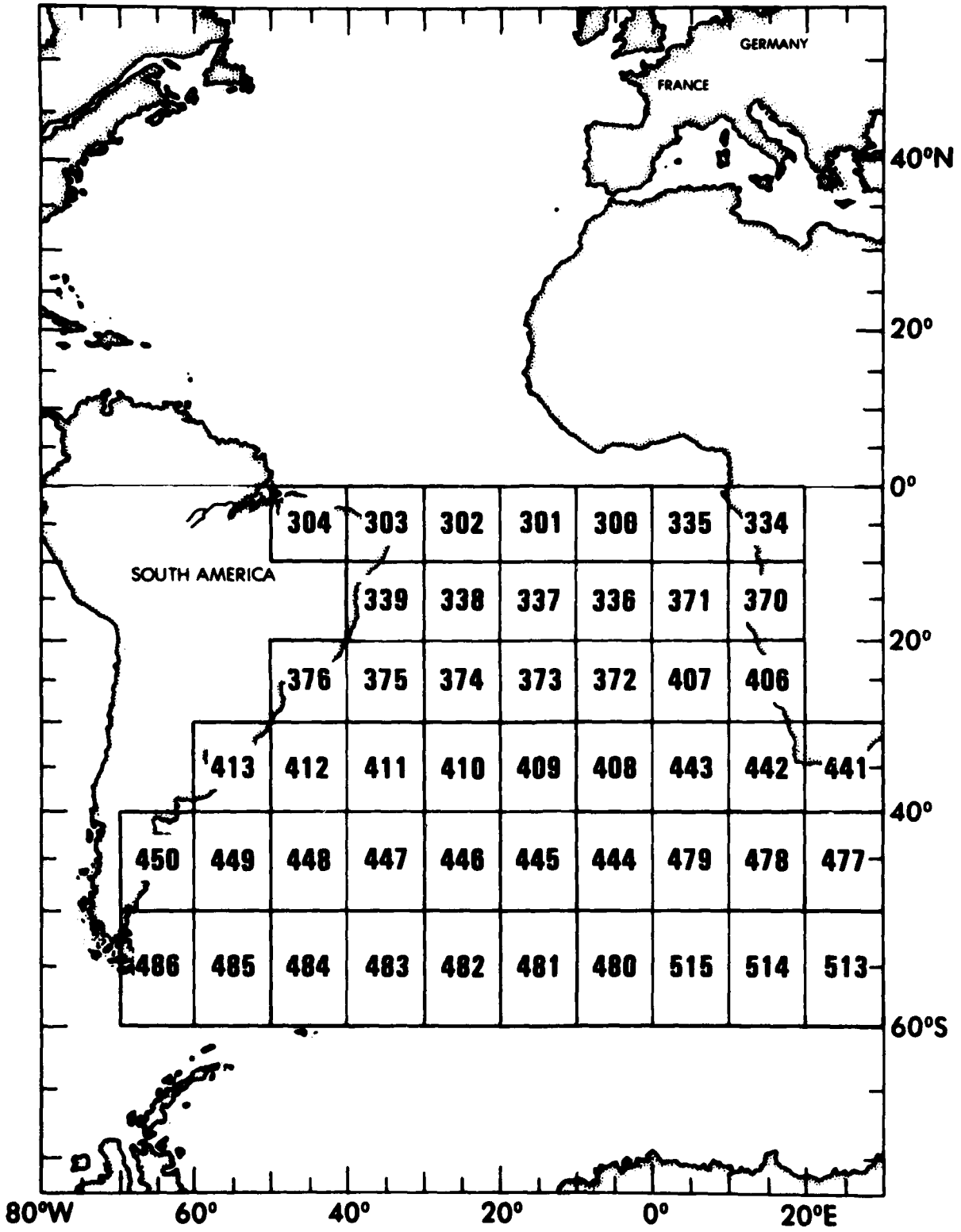

Figure 1. South Atlantic Marsden Squares

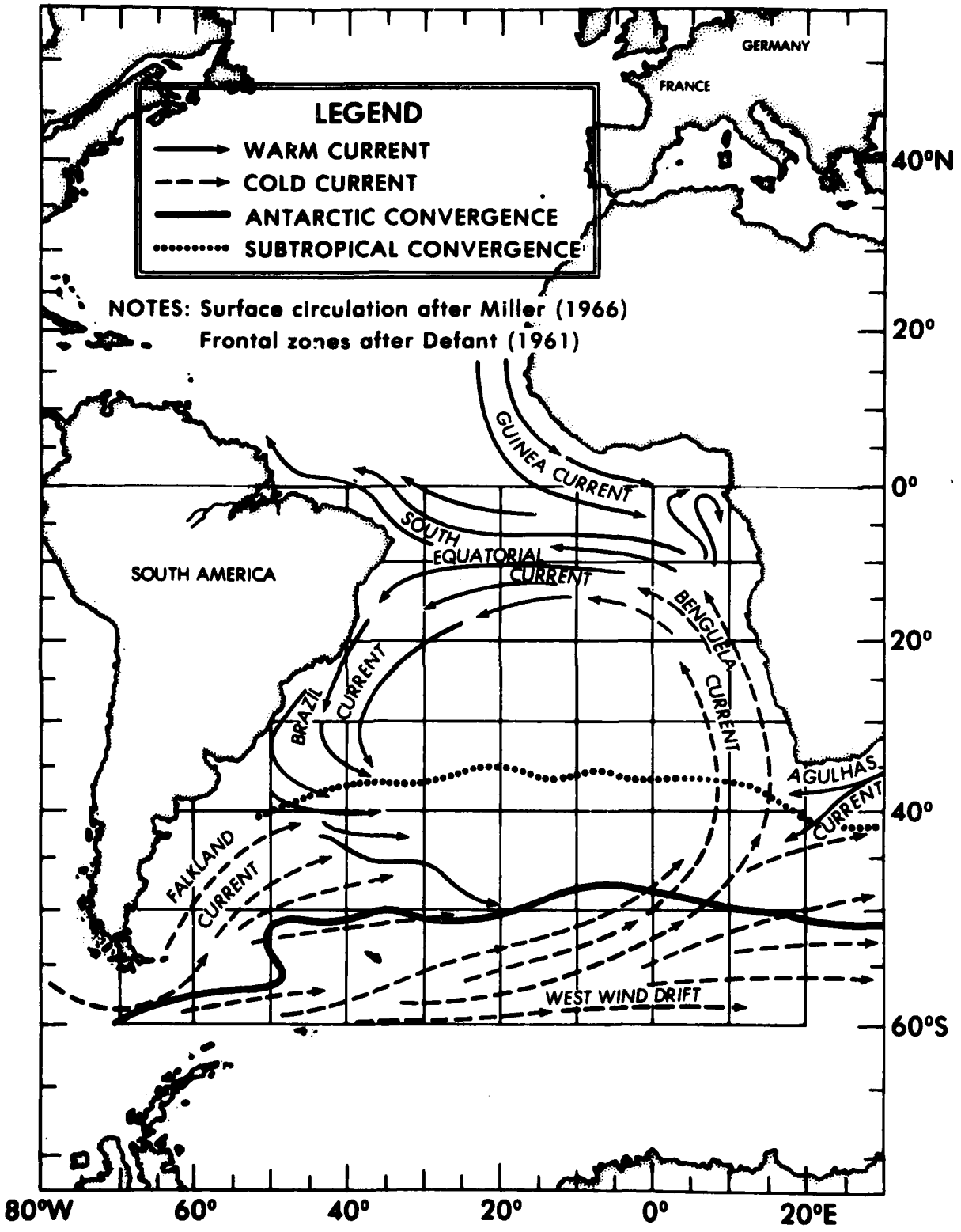

Figure 2. Surface Circulation and Frontal Zones in the South Atlantic Ocean

Figure 3 shows the core depth and circulation pattern of Antarctic Intermediate Water (AAIW) as it flows north from the Antarctic Convergence into the South Atlantic Ocean. The flowpaths shown on Figure 3 are similar to those shown by Defant (1961). The core depths of the AAIW salinity minimum are primarily from Wust (1936). However, the AAIW low salinity core depths shown on Figure 3 have been modified using data collected during the Canadian HUDSON-70 Exercise (Duedall and Coote, 1972) and data collected during the Geochemical Ocean Station (GEOSECS) Program during 1972-1973. The HUDSON-70 data lies only in the western South Atlantic. The GEOSECS data comes from both sides of the Mid-Atlantic Ridge, and is reported in detail by Broecker and Takahasi (1981) for intermediate depths in the South Atlantic Ocean. Similar AAIW core depths to those shown on Figure 3 are given by Menzel and Ryther (1968) for the western South Atlantic between 9°S and 36°S latitude and for the entire western South Atlantic by Buscaglia (1971). All these sources indicate that the major northward flow of AAIW in the South Atlantic lies west of the Mid-Atlantic Ridge.

Figure 4 shows the southward flow of Mediterranean Intermediate Water (MIW) from the North Atlantic into the South Atlantic Ocean. The depths of the MIW high salinity core are from the research of Wust as reported by Defant (1961), but are similar to those given by Sverdrup, Johnson, and Fleming (1942). The MIW core sinks by about 1000 m as it flows south from the Equatorial Atlantic toward the South Atlantic Subtropical Convergence zone. Although MIW flow apparently is more pronounced west of the Mid-Atlantic Ridge in the region north of the Subtropical Convergence zone, the MIW high salinity core is also found east of the Mid-Atlantic Ridge, particularly in the region south of the Subtropical Convergence zone. South of about 40°S latitude, the depth of the MIW core rises rapidly due to the influence of the Antarctic Convergence. As pointed out for the western South Atlantic Ocean (south of about 20°S latitude) by Reid, Nowlin, and Patzert (1977), the top of the MIW high salinity layer frequently intermixes with the bottom of the AAIW low salinity layer.

Figure 5 shows the northward flow of the low salinity Antarctic Bottom Water (AABW) core at depths greater than 3500 m. As was the case with AAIW, the main northward flow of AABW occurs west of the Mid-Atlantic Ridge over the Argentine and Brazil Plains. The northward flow of this near-bottom low salinity core is described in detail by Wust (1957) and Wright (1971). Both works indicate that the primary northward flow of AABW is west of the Mid-Atlantic Ridge in both the South Atlantic Ocean and the North Atlantic Ocean. Northward flow of AABW in the western South Atlantic Ocean is also discussed by Reid, Nowlin, and Patzert (1977), who indicate that the bottom of the southward flowing MIW layer frequently intermixes with the top of the northward flowing AABW layer, particularly in the region south of about 25°S latitude.

III. OBSERVATIONS DEEPER THAN THE DEEP SOUND CHANNEL AXIS

Figure 6 shows the number of austral summer observations per one-degree square deeper than the deep sound channel (DSC) axis. This figure is based on data from the files of the NORDA Numerical Modeling Division. Other existing summer data include:

- HUDSON-70 Exercise Nansen cast data extending from the surface to the bottom collected in late December 1969 and January 1970 and listed in Bowers (1971) and Duedall and Coote (1972). The late December 1969 data extends southward along about 30°W from the Equator to 40°S. The January 1970 data lies east of 45°W either along 30°W between 49°S and 55°S or farther to the west over the Argentine Plain.

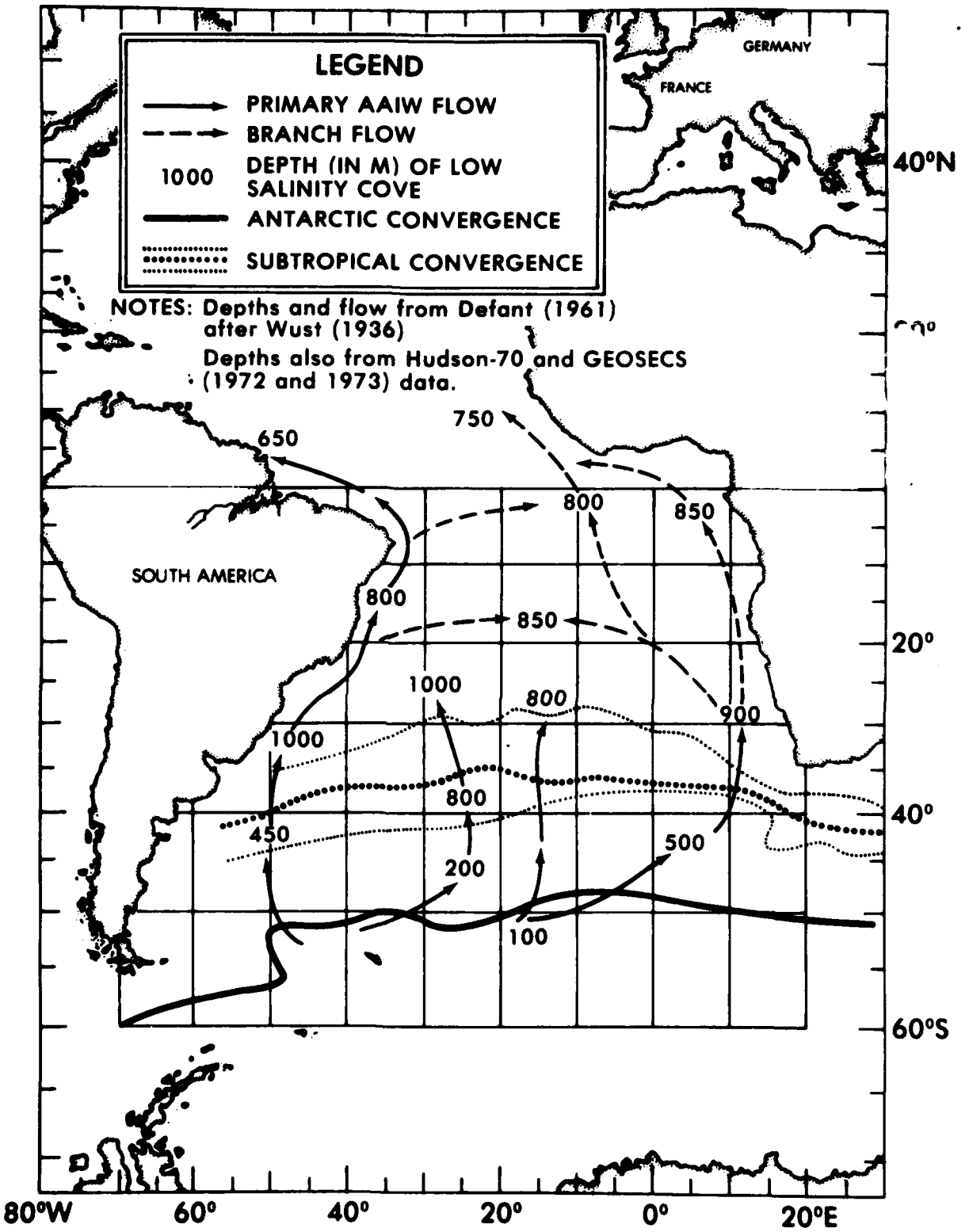

Figure 3. Antarctic Intermediate Water (AAIW) Flow in the South Atlantic Ocean

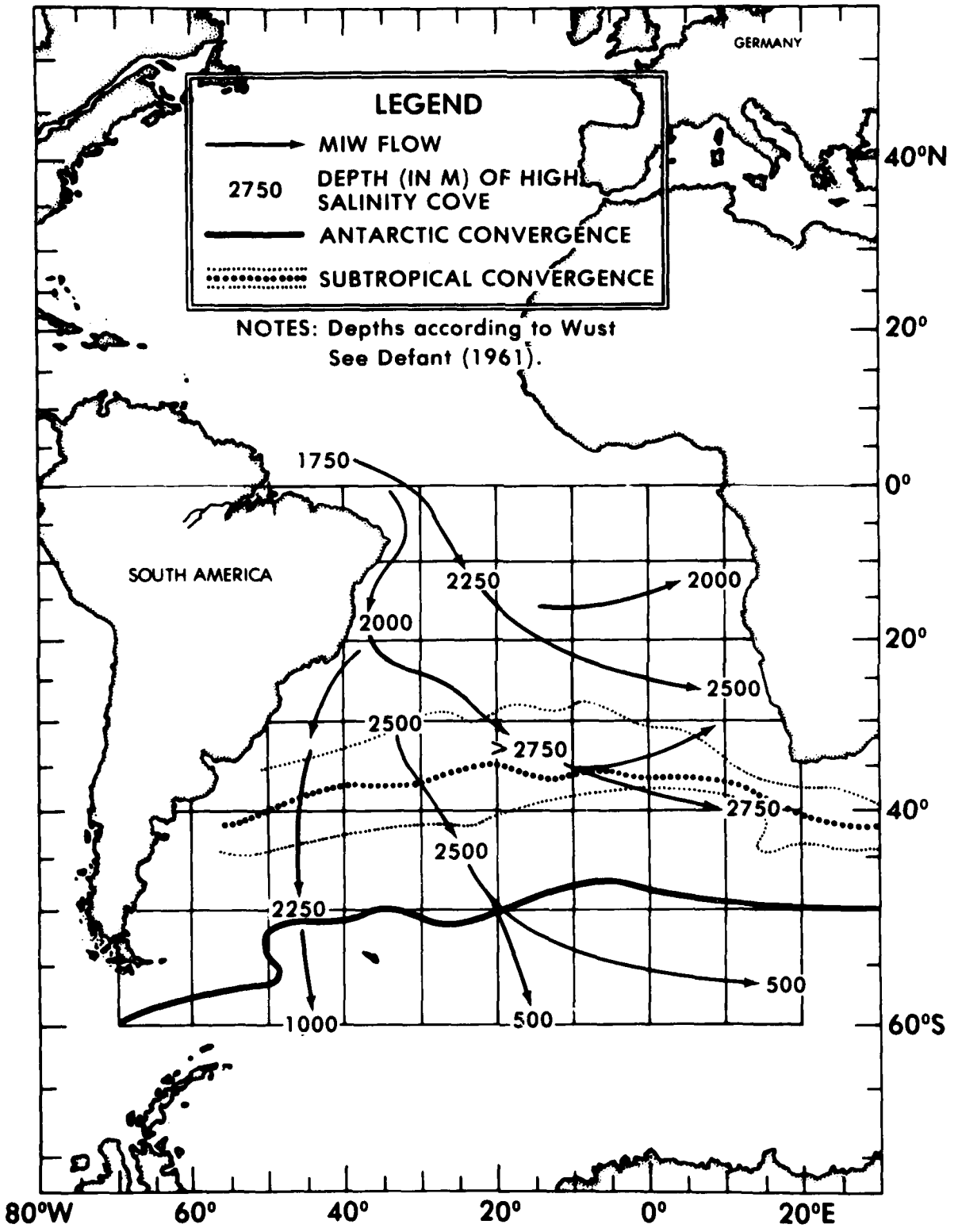

Figure 4. Mediterranean Intermediate Water (MIW) Flow in the South Atlantic Ocean

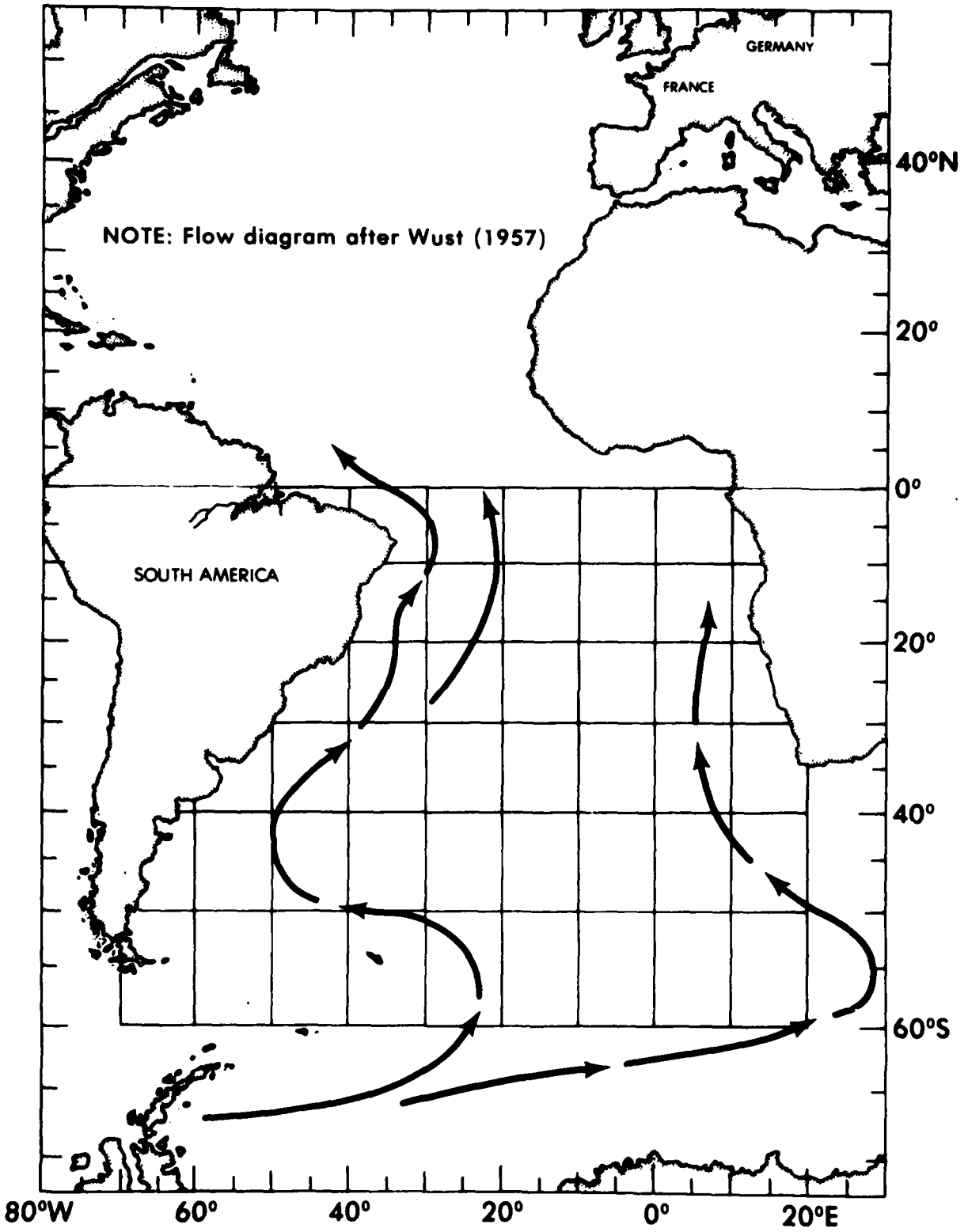

Figure 5. Antarctic Bottom Water (AABW) Flow in the South Atlantic Ocean

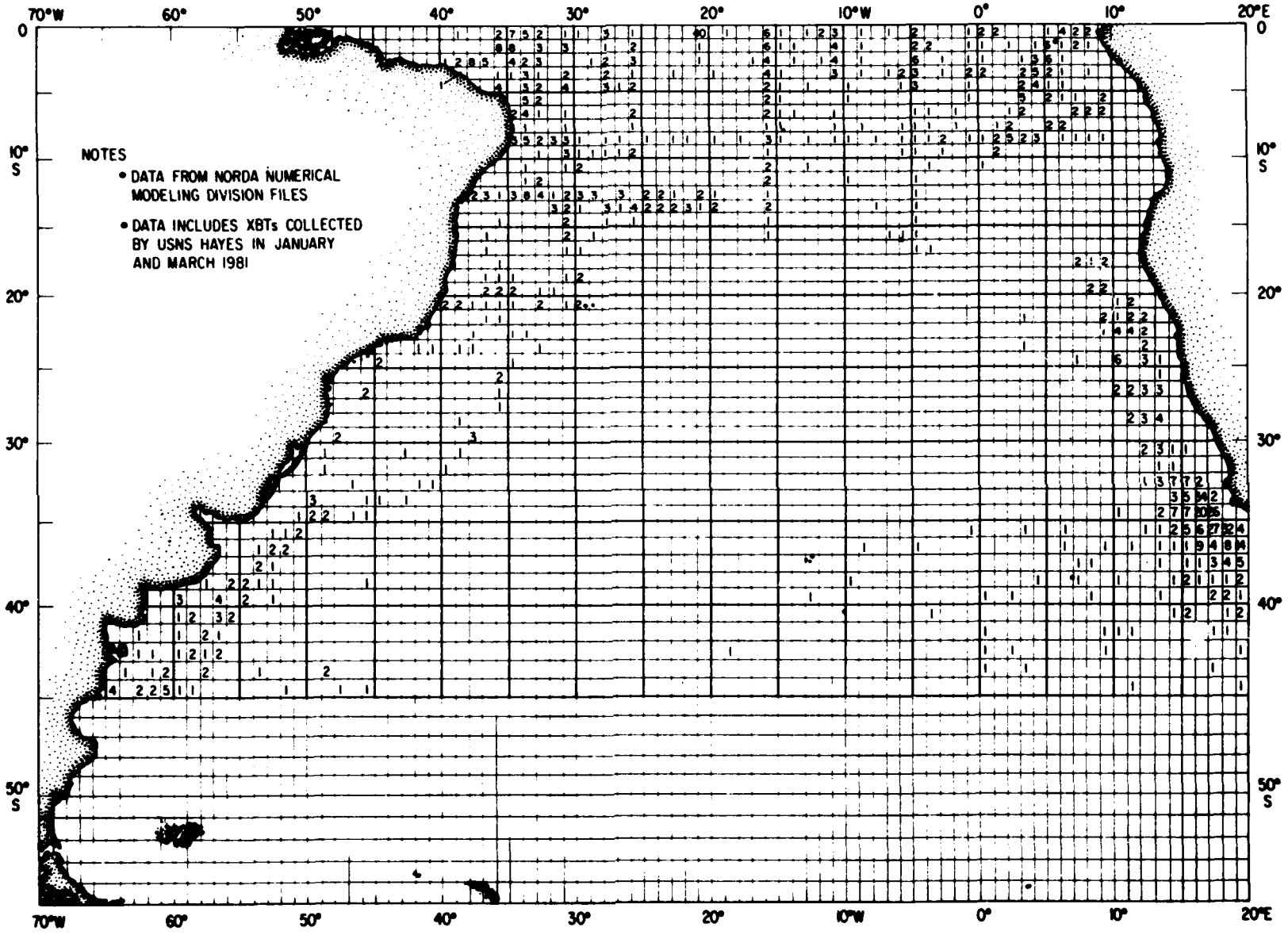

Figure 6. Number of Austral Summer (Jan-Mar) Observations Deeper than the Depth of the DSC Axis

- GEOSECS program data tken in the eastern South Atlantic during February-March 1973 and in the western South Atlantic during December 1972. These data are listed in Broecker and Ostlund (1979). Although neither HUDSON-70 Exercise nor GEOSECS program data are shown on Figure 6, USNS HAYES T-5 expendable bathythermograph (XBT) data from January and March 1981 are shown.

Figure 7 shows the number of austral winter observations per one degree, and are exclusively from the files of the NORDA Numerical Modeling Division. Due to cold austral winter conditions along both the South American and African coasts, the data shown on Figure 7 frequently include shallow observations with surface-to-bottom positive sound speed gradients. This situation is most common between 35°S and 45°S off the Argentina coast and south of 20°S off the South African coast.

Further investigation has indicated that considerable other data deeper than the depth of the DSC axis exist in the western South Atlantic north of 55°S that are not in the NORDA Numerical Modeling Division files and are not shown on Figure 6 or Figure 7. These data include the following:

- Austral winter conductivity-temperature-depth (CTD) profiles and T-7 XBT profiles collected south of 40°S and west of 45°W by the R/V ATLANTIS II during August-September 1980. These data generally lie in Marsden squares 449, 484, and 485 (see Fig. 1) and have been published by Georgi, Piola, and Galbraith (1981) and by Piola, Georgi, and Stalcup (1981).

- Austral summer salinity-temperature depth (STD) profiles collected in Marsden square 412 by R/V CONRAD during March 1981 that have been published by Georgi, Amos, Draganovic, and Raymer (1979).

- Austral winter T-5 XBT profiles collected in Marsden square 339 by R/V ALTE CAMARA during July 1981. These data are available from either the author or the NRL Acoustics Division.

- Austral summer T-5 XBT and conductivity-temperature-depth-sound velocity (CTD/SV) profiles collected by the USNS HAYES during February 1981 south of 35°S and west of 40°W. These data also are available from either the author or the NRL Acoustics Division.

The USNS HAYES completed an austral summer cruise (January 1982) north of the Victoria Seamounts taking T-5 XBTs in Marsden Squares 303, 338, and 339. The temperature printouts of these data have been provided to the author by Norman Cherkis of the NRL Acoustics Division (personal communication) and will be converted into sound speed profiles at request and distributed to interested parties as required. It is the opinion of the author that further investigations will uncover additional data from both austral summer and austral winter that are not currently available in the NORDA data files for the entire South Atlantic Ocean.

IV. WESTERN SOUTH ATLANTIC SOUND SPEED CROSS-SECTIONS

Figure 8 shows the location of the five western South Atlantic sound speed cross-sections investigated in this report. These cross-sections are identified on Figure 8 according to location and season. Cross-sections A and C are for both austral summer and austral winter; cross-section B is for austral winter only. Cross-section A extends diagonally from 45°S, 52°W across the Argentine and Brazil Plains to the Equator at 15°W. Cross-section B extends due north along 30°30'W from 45°S to the Equator. Cross-section C extends due north along 46°30'W from 50°S

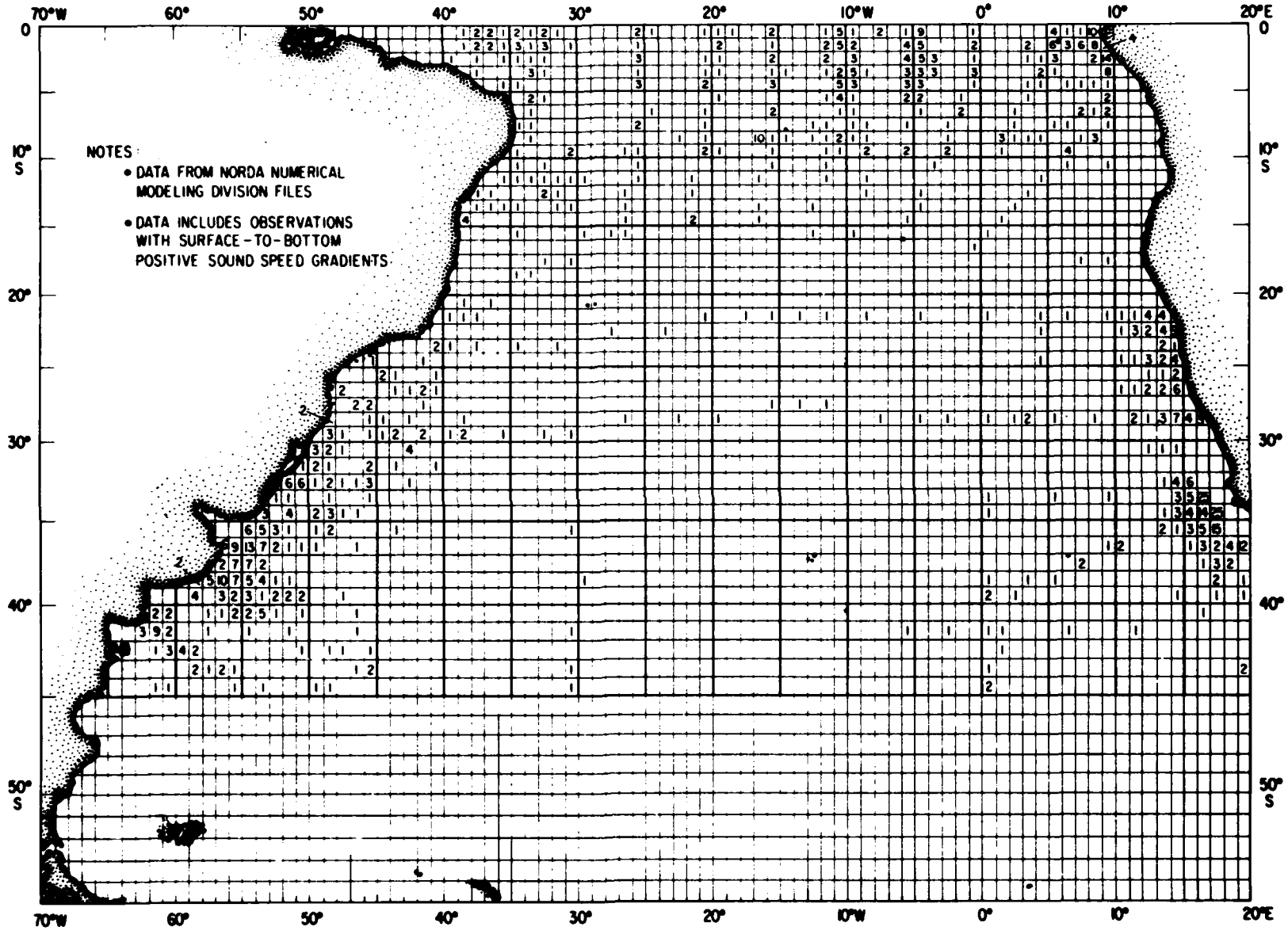

Figure 7. Number of Austral Winter (Jul-Sep) Observations Deeper than the Depth of the DSC Axis

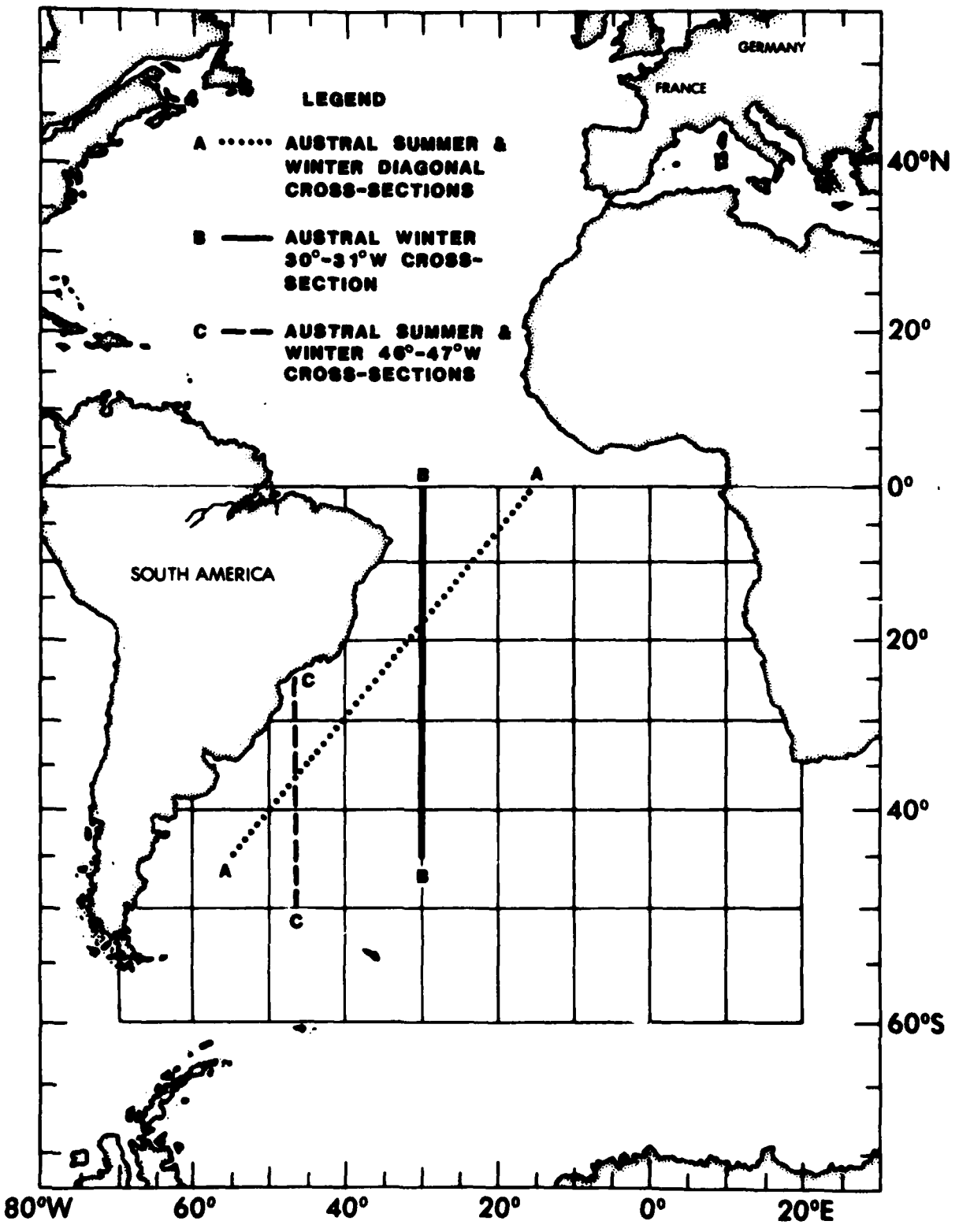

Figure 8. Location of Western South Atlantic Sound Speed Cross-Sections

across the Argentine Plain to the Brazil coast (about 24°S). Bathymetry along all five cross-sections was mainly derived from the NRL Acoustic Division chart entitled "Bathymetry of the South Atlantic" (Perry, 1980). However, when necessary, bathymetry from this chart has been supplemented with Naval Oceanographic Office (NAVOCEANO) Standard Navy Ocean Area charts SA-1, SA-3, SA-3A, SA-5, and SA-5A and from depth observations made when each individual profile was collected. All bathymetry used in the five cross-sections has been corrected using the tables of Matthews (1939).

V. SOUND SPEED STRUCTURE ALONG CROSS-SECTION A

The sound speed profiles shown on the summer diagonal cross-section (Fig. 9) and the winter diagonal cross-section (Fig. 10) are identified in Tables 1 and 2, respectively. Summer profiles 3 through 11, 14, and 15 represent T-5 XBTs collected by the USNS HAYES during either January or March 1981. These XBTs were converted into sound speed profiles by the author using the Mackenzie equation and nearby historical summer salinity data. All sound speed profiles used to construct Figures 9 and 10 were extended to correct bottom depth using nearby summer or winter data, as available.

Cross-section A starts at the southern edge of the South Atlantic Subtropical Convergence zone, but considerably north of the Antarctic Convergence (see Fig. 2). In the near-surface layer, cross-section A is under the influence of the cold Falkland Current over the first 500-600 nmi during both summer and winter. Both diagonal cross-sections leave the influence of the Subtropical Convergence zone at about 32°S, 40°W. During both summer and winter, the Subtropical Convergence zone causes a rapid deepening to the north of both the depth of the DSC axis and critical depth. This rapid increase is most pronounced within the first 600 nmi on the winter diagonal (Fig. 10). Over the first 600 nmi, during the winter, the depth of the DSC axis increases from 250 m (profile 1) to 1020 m (profile 4), and critical depth increases from 620 m (profile 1) to 4520 m (profile 4). All four of these winter profiles lie south of the Rio Grande Plateau over the Argentine Plain.

In the near-surface layer, winter cross-section A (Fig. 10) is far more complicated oceanographically than summer cross-section A (Fig. 9), particularly in the area south of about 35°S latitude over the Argentine Plain and the southern slope of the Rio Grande Plateau. As shown by Cheney and Marsh (1981), this portion of the western South Atlantic is a region of intense mesoscale variability in which eddy formation can be expected throughout the year. Eddy formation is not apparent along summer cross-section A, but does occur along winter cross-section A (Fig. 10). Winter profile 2 (at a range of 200 nmi) is clearly a different type of sound speed profile than either winter profile 1 (range of 0 nmi) or winter profile 3 (range of 350 nmi). This difference probably is the result of a warm, anticyclonic eddy formed south of the Subtropical Convergence during September 1962. This warm eddy most likely represents an intrusion of the warmer Brazil Current into the colder, near-surface regime of the Falkland Current. As indicated in Table 2, winter profiles 2 and 3 were taken only four days apart on 4 and 8 September 1962. Winter profile 1 was also taken during September 1962. As shown in Figure 17, winter profile 3 is of an entirely different shape than either profiles 1 or 2, and more closely resembles winter profiles 4 and 6, both taken during July 1960 within the warmer regime of the Brazil Current.

The depth of the DSC axis along both the summer and winter cross-sections roughly corresponds with the depth of the AAIW salinity minimum. As shown on Figure 3, the AAIW low salinity core lies at a maximum depth of about 1000 m for

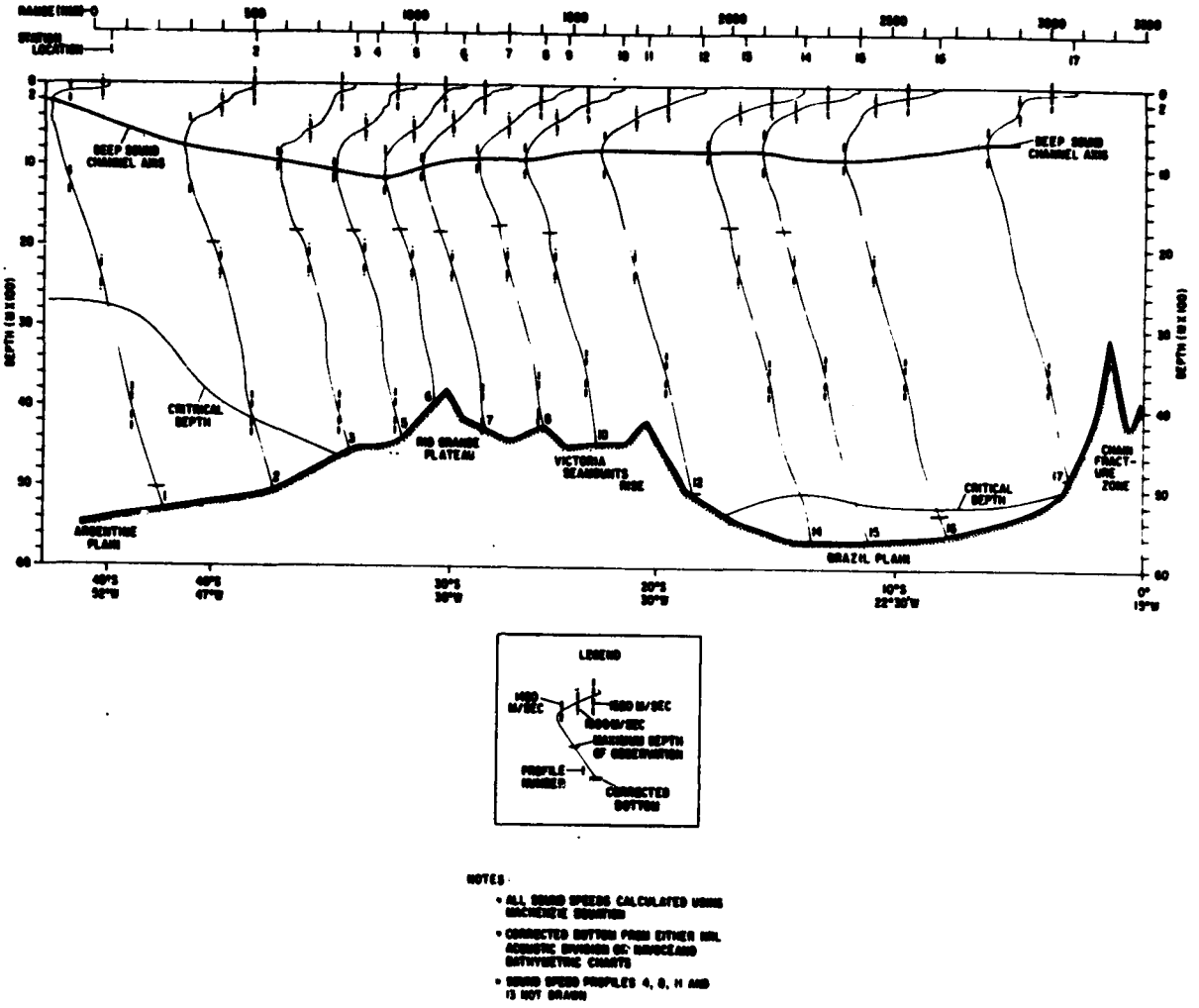

Figure 9. Sound Speed Cross-Section A for Austral Summer

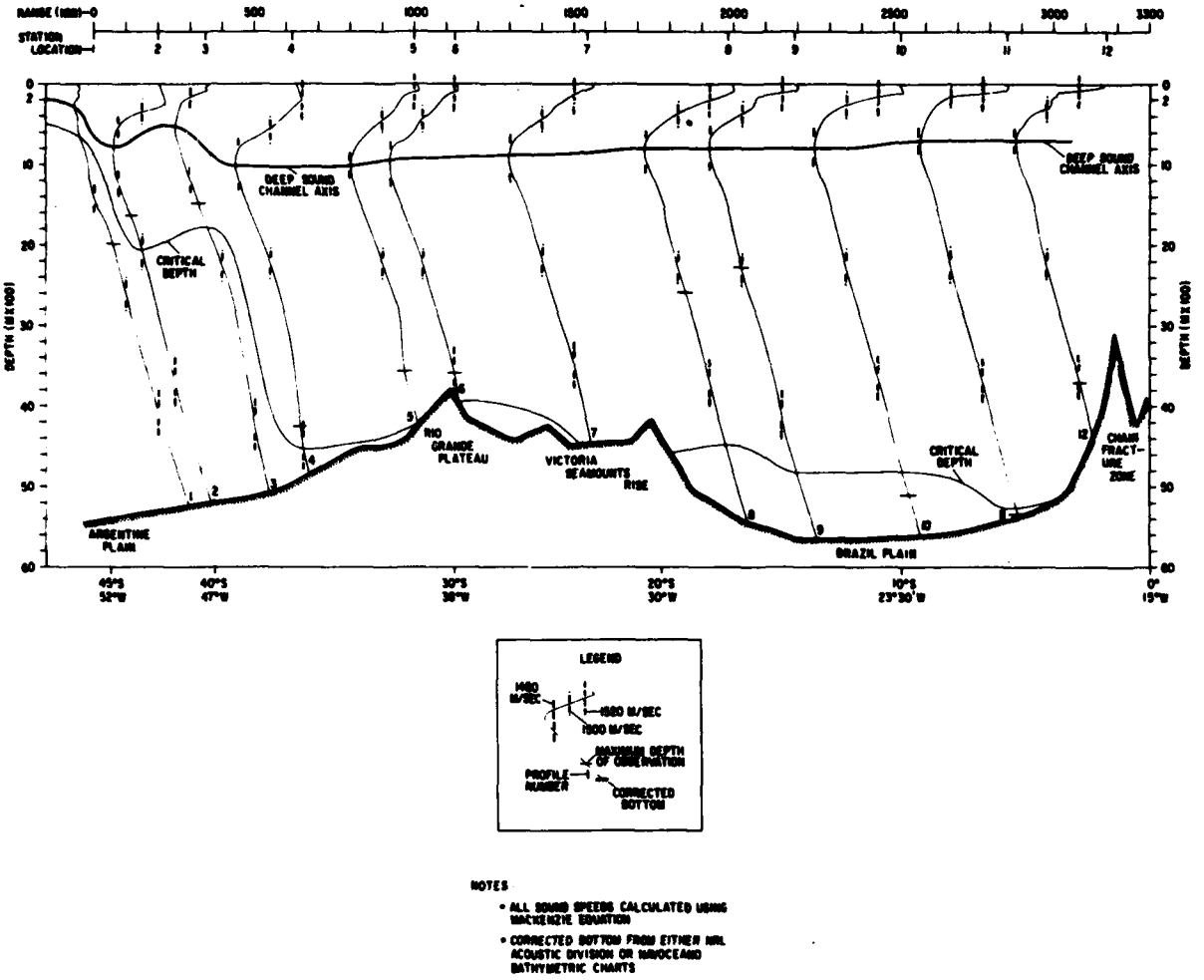

Figure 10. Sound Speed Cross-Section A for Austral Winter

Table 1. Identification of Profiles for Summer Cross-Section A

PROFILE NUMBER	LAT (°S)	LONG (°W)	DATE	MAX DEPTH (M)	RANGE FROM 45°S, 52°W (NM)	COR. BOTTOM DEPTH (M)
1	44°00'	51°00'	21 Mar 1959	5032	80	5370
2	38°00'	45°50'	4 Mar 1961	1970	510	5110
3	33°17'	42°56'	24 Jan 1981	1821	825	4512
4	32°50'	41°18'	24 Jan 1981	1813	890	4502
5	31°13'	39°29'	23 Jan 1981	1821	1010	4245
6	29°40'	37°42'	22 Jan 1981	1806	1160	4114
7	27°53'	36°56'	22 Jan 1981	1825	1300	4409
8	25°59'	35°03'	21 Jan 1981	1815	1415	4239
9	23°48'	34°02'	21 Jan 1981	1737	1490	4475
10	20°31'	32°31'	20 Jan 1981	1814	1660	4438
11	19°18'	31°58'	20 Jan 1981	1616	1740	4165
12	18°00'	29°00'	19 Mar 1959	5065	1910	5111
13	15°49'	28°40'	19 Mar 1959	5124	2020	5397
14	14°02'	25°01'	18 Mar 1981	1742	2230	5644
15	12°02'	23°20'	14 Mar 1981	1778	2400	5659
16	8°16'	21°02'	17 Mar 1957	5310	2650	5386
17	2°40'	16°31'	2 Jan 1927	4345	3070	4864

Table 2. Identification of Profiles for Winter Cross-Section A

PROFILE NUMBER	LAT (°S)	LONG (°W)	DATE	MAX DEPTH (M)	RANGE FROM 45°S, 52°W (NM)	COR. BOTTOM DEPTH (M)
1	45°38'	52°50'	23 Sep 1962	1992	0	5398
2	42°04'	50°05'	4 Sep 1962	1635	200	4888
3	40°53'	46°33'	8 Sep 1962	1483	350	5207
4	36°30'	46°43'	12 Jul 1960	4360	620	4512
5	31°00'	40°04'	7 Jul 1960	3582	1000	4209
6	29°51'	38°00'	7 Jul 1960	3704	1130	4005
7	23°36'	31°48'	7 Jul 1926	4626	1540	5079
8	16°20'	29°17'	15 Aug 1963	2598	1980	4774
9	14°03'	26°24'	14 Aug 1963	2355	2190	5057
10	11°04'	21°08'	12 Sep 1963	5112	2520	5202
11	5°01'	19°57'	10 Sep 1963	5371	2850	5524
12	2°01'	15°01'	9 Sep 1963	3700	3160	3066

both the summer and winter diagonals. The deepest depth for the DSC axis along cross-section A is for summer profile 6, where the depth of the DSC axis lies at 1160 m, nearly 300 m deeper than the depth of the AAIW low salinity core.

The effects of the MIW high salinity core are observable on most of the profiles used to construct summer cross-section A (Fig. 9) and winter cross section A (Fig. 10). As indicated on Figure 4, the MIW core was found at depths between about 1750 m and 2500 m along both cross-sections. The MIW core generally caused higher sound speed and sound speed perturbations. These perturbations are particularly noticeable along summer cross-section A for profiles over the Rio Grande Plateau and Victoria Seamounts Rise (i.e., profiles 3 through 10), but perturbations caused by the MIW layer are also noticeable over both the Brazil Plain and Argentine Plain. Similar perturbations are also evident along winter cross-section A. As noted by Buscaglia (1971), the top of the MIW layer frequently intermixes with the bottom of the AAIW layer throughout the western South Atlantic Ocean. This intermixing may be present for many of the sound speed irregularities found on both Figures 9 and 10 at depths between about 1000 m and 2000 m.

AABW effects on sound speed profiles also are apparent on both Figures 9 and 10. These effects are particularly noticeable for profiles over the Rio Grande Plateau and to the south of the Rio Grande Plateau over the Argentine Plain. However, some AABW effects on near-bottom sound speed gradients are apparent over the Brazil Plain just north of the Victoria Seamounts Rise (profile 14 on Fig. 9). Farther to the north, an AABW effect on the near-bottom sound speed gradient is apparent just south of the CHAIN Fracture Zone (profile 17 on Fig. 9). Similar near-bottom effects are not as apparent over the Brazil Plain on the winter diagonal (Fig. 10), probably due to the positions of the winter sound speed profiles. However, in terms of temperature and salinity, AABW is present over the Brazil Plain during both seasons.

VI. SOUND SPEED STRUCTURE ALONG CROSS-SECTION B

The sound speed profiles shown in Figure 11 are identified in Table 3 and represent the best austral winter data available north of 45°S between 29°W and 31°W. As indicated on Figure 7, there is an extreme paucity of winter data between 29°W and 30°W south of 30°S. However, as shown on Figure 6, there is absolutely no available summer data that corresponds to the location of cross-section B.

Figure 11 starts just south of the South Atlantic Subtropical Convergence zone but north of the Antarctic Convergence in a cold water regime influenced in the near-surface layer by mixing of the cold Falkland Current with warmer waters of the Brazil Current (see Fig. 2). Profiles 1, 2, and 3 are located south of the southern limit of the Subtropical Convergence zone while profiles 4, 5, and 6 lie within the zone itself. Actually, profile 6 lies on the northern edge of the Subtropical Convergence zone and displays a surface sound speed of nearly 1520 m/sec caused by the warming influence of the Brazil Current. North of profile 6 (29°15'S, 30°30'W), profiles 7 through 14 show surface sound speeds between 1530 m/sec and 1540 m/sec and have sonic layers that are considerably shallower than found on profiles farther to the south. Although the first five sound speed profiles used to construct Figure 11 were collected during September 1958 (see Table 3), there are no eddies apparent in the first 500 nmi along 30°W. However, eddies could be expected to form during both summer and winter within the limits of the Subtropical Convergence zone.

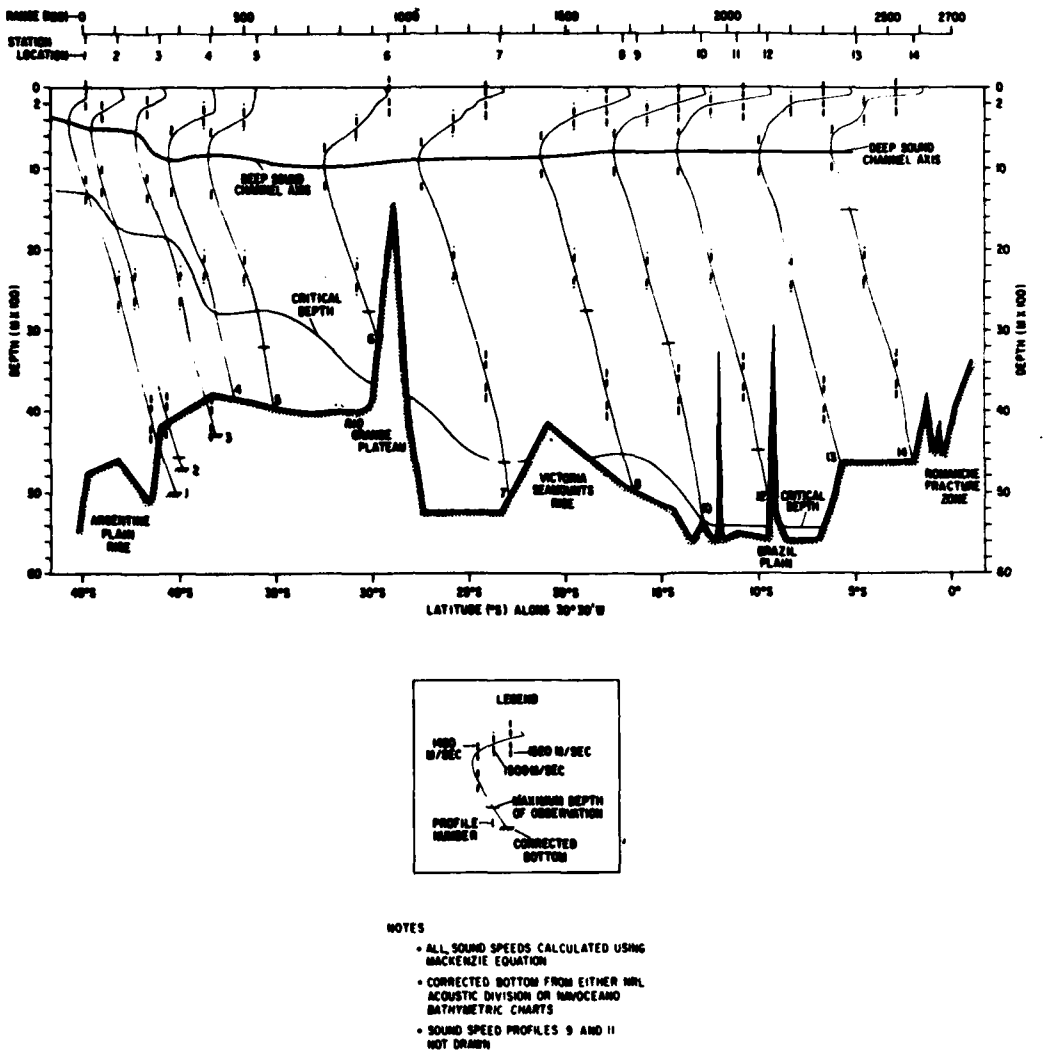

Figure 11. Sound Speed Cross-Section B for Austral Winter

Table 3. Identification of Profiles for Winter Cross-Section B

PROFILE NUMBER	LAT (°S)	LONG (°W)	DATE	MAX. DEPTH (M)	RANGE FROM 45°S (NMI)	COR. BOTTOM DEPTH (M)
1	44°52'	30°21'	12 Sep 1958	4763	8	4898
2	43°11'	30°15'	13 Sep 1958	4562	110	4579
3	41°26'	30°00'	14 Sep 1958	3962	240	4163
4	38°32'	29°59'	15 Sep 1958	3784	400	4248
5	35°58'	30°01'	30 Sep 1958	3205	540	4300
6	29°15'	30°00'	20 Aug 1925	2757	950	4001
7	23°36'	31°48'	7 Jul 1926	4626	1300	5081
8	17°04'	30°41'	16 Aug 1963	2753	1680	4777
9	16°20'	29°17'	15 Aug 1963	2598	1720	4771
10	13°00'	30°16'	21 Aug 1959	3154	1920	5232
11	11°06'	30°42'	23 Aug 1959	2962	2030	5334
12	9°32'	30°01'	23 Jul 1926	4475	2125	5412
13	5°08'	32°19'	24 Jul 1911	4592	2400	4609
14	1°50'	30°26'	2 Jul 1911	1500	2580	4495

Both critical depth and the depth of the DSC axis increase rapidly to the north in the region just south of the Rio Grande Plateau (i.e., south of 29°-30°S latitude). The northward increase in critical depth continues over the Brazil Plain until a maximum critical depth of 5420 m occurs on profile 13 at about 5°S latitude. The depth of the DSC axis varies to the north from a minimum of 400 m at 45°S (profile 1) to a maximum of 975 m at 29°S (profile 6). North of about 15°S, the depth of the DSC axis is relatively constant at 800 m. Along the entire cross-section, the depth of the DSC axis lies within 100 m to 200 m of the depth of the low salinity AAIW core. The AAIW core depth varies from 300-600 m on profile 1 to about 900 m on profile 6. Both of these profiles lie south of the Rio Grande Plateau. North of the Rio Grande Plateau, the AAIW core lies between 800 m and 900 m south of 10°S latitude. North of 10°S latitude, the AAIW core depth becomes shallower than 800 m, as is also indicated on Figure 3. This is substantiated by an AAIW salinity minimum of 600 m for profile 14 (located at 1°50'S, 30°26'W). However, even for profile 14, the depth of the DSC axis lies at 800 m.

The effects of the MIW high salinity core are apparent on many of the profiles used to construct Figure 11. The MIW core was found between 2300 m and 2500 m for profiles 1 through 8, but occurred at 1580 m for profile 10 and at depths shallower than 2000 m for profiles 12, 13, and 14. In all cases, MIW caused somewhat higher sound speeds than would have been found in the absence of the warmer, high salinity core and frequently led to the formation of a sound speed perturbation. This perturbation is apparent for profiles on either side of the Rio Grande Plateau and the Victoria Seamounts Rise, but is most noticeable on profiles 4, 12 and 13. It should be noted that the top of the southward flowing MIW layer can and does mix with the bottom of the northward flowing AAIW layer throughout the western South Atlantic Ocean. This intermixing has been observed along 30°W longitude by Duedall and Coote (1972) and throughout the western South Atlantic Ocean by Buscaglia (1971). In the presence of this intermixing, the MIW sound speed perturbation can disappear. The effects of the near-bottom AABW low salinity minimum are also apparent on many of the sound speed profiles used to construct Figure 11. As was expected, AABW caused lower sound speeds and modified sound speed gradients just above the bottom south of the Rio Grande Plateau and over the Brazil Plain. These effects are apparent on profiles 4 and 5 (just south of the Rio Grande Plateau), on profiles 7 and 10 (over the Brazil Plain), and on profile 14 (at 1°50'S, near the Romanche Fracture Zone). Profile 7 lies just north of the Vema Channel, a principal near-bottom gap on the western side of the Rio Grande Plateau through which AABW passes as it moves northward in the western South Atlantic Ocean. AABW flow through and in the environs of the Vema Channel is discussed in detail by Johnson, McDowell, Sullivan, and Biscayne (1976). The presence of AABW would also be expected in the region of the Romanche Fracture Zone as the near-bottom flow moves to the northwest between the Brazil coast and the Mid-Atlantic Ridge (see Fig. 5). In this region, some intermixing between the bottom of the MIW layer and the top of the AABW layer might also be expected. Such an intermixing has been observed over the Argentine Plain by Reid, Nowlin, and Patzert (1977), as will be discussed further in a following section.

VII. SOUND SPEED STRUCTURE ALONG CROSS-SECTION C

The sound speed profiles used to construct Figure 12 (summer) and Figure 13 (winter) are identified in Tables 4 and 5, respectively. As shown in Figures 6 and 7, the data used to construct the summer and winter sound speed cross-sections along 46°30'W represent the best and most eastern data available over the Argentine Plain between 45°S latitude and the Brazil coast. Both cross-sections start within the South Atlantic Subtropical Convergence zone but north of the Antarctic Convergence at about 50°S latitude (see Fig. 2). Both cross-sections begin within the cold

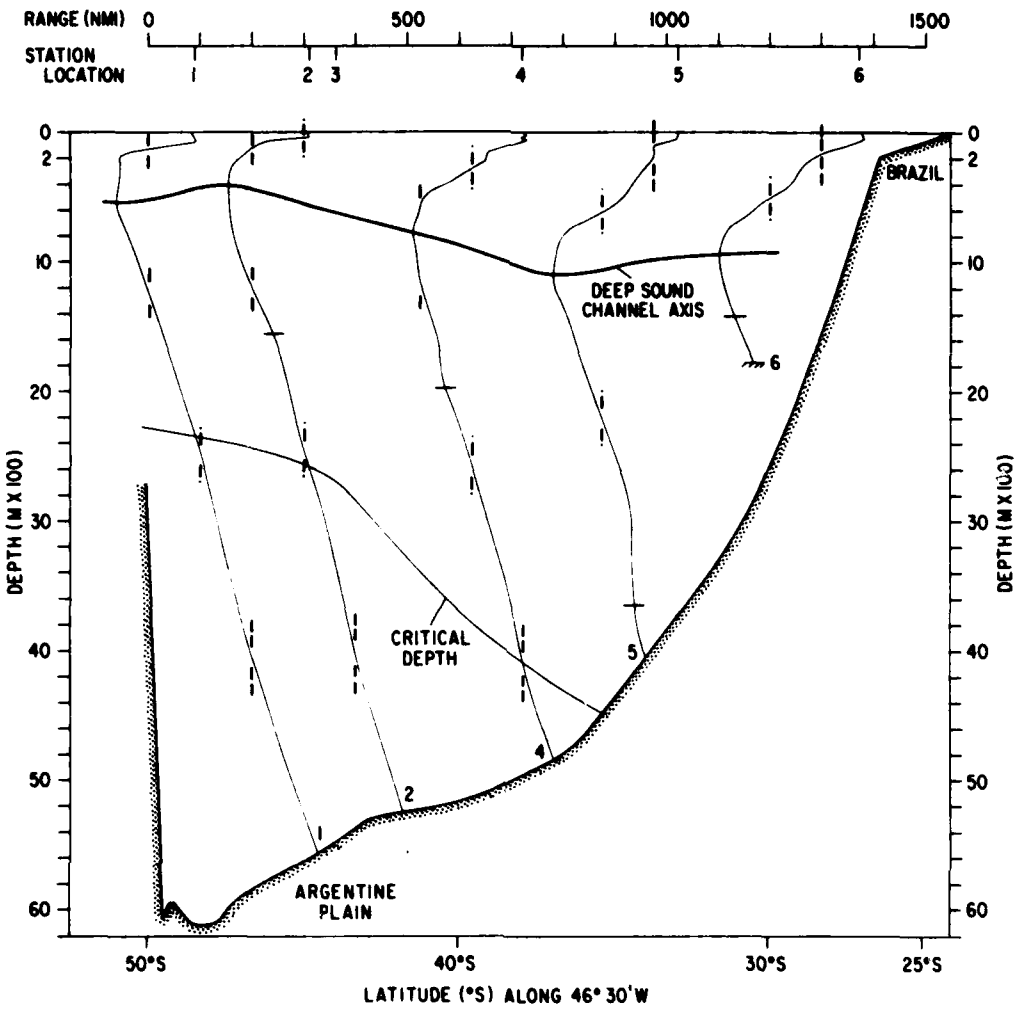

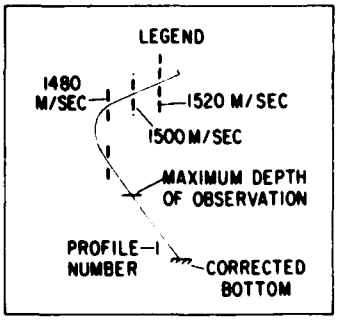

NOTES:

- ALL SOUND SPEEDS CALCULATED USING MACKENZIE EQUATION
- CORRECTED BOTTOM FROM EITHER NRL ACOUSTIC DIVISION OR NAVOCEANO BATHYMETRIC CHARTS
- SOUND SPEED PROFILE 3 NOT DRAWN

Figure 12. Sound Speed Cross-Section C for Austral Summer

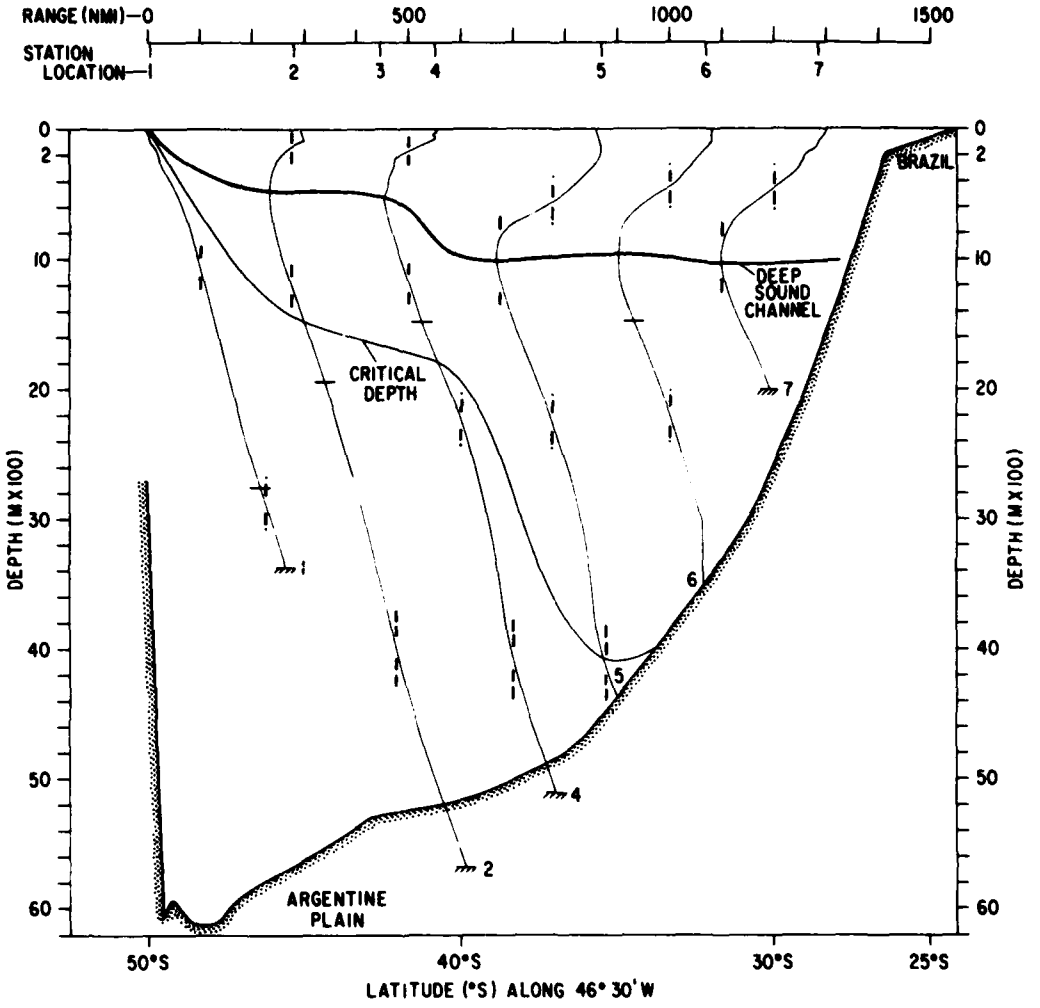

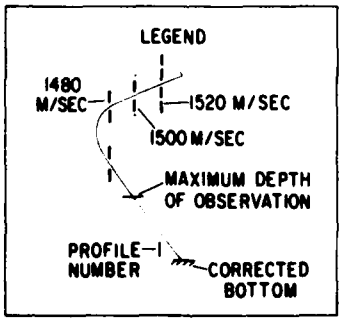

NOTES:

- ALL SOUND SPEEDS CALCULATED USING MACKENZIE EQUATION
- CORRECTED BOTTOM FROM EITHER NRL ACOUSTIC DIVISION OR NAVOCEANO BATHYMETRIC CHARTS
- SOUND SPEED PROFILE 3 NOT DRAWN

Figure 13. Sound Speed Cross-Section C for Austral Winter

Table 4. Identification of Profiles for Summer Cross-Section C

PROFILE NUMBER	LAT (°S)	LONG (°W)	DATE	MAX. DEPTH (M)	RANGE FROM 50°S (NMI)	COR. BOTTOM DEPTH (M)
1	48°28'	47°22'	18 Mar 1959	5640	90	5786
2	45°08'	47°14'	31 Mar 1964	1652	310	5122
3	43°56'	48°06'	20 Mar 1959	4700	360	5010
4	38°00'	45°50'	14 Mar 1961	1970	720	5110
5	32°56'	46°07'	15 Mar 1967	3739	1029	3965
6	27°09'	46°10'	25 Mar 1967	1406	1370	1794

Table 5. Identification of Profiles for Winter Cross-Section C

PROFILE NUMBER	LAT (°S)	LONG (°W)	DATE	MAX. DEPTH (M)	RANGE FROM 50°S (NMI)	COR. BOTTOM DEPTH (M)
1	49°48'	40°03'	12 Aug 1963	2752	10	3370
2	45°17'	47°31'	24 Aug 1962	1941	280	5676
3	43°04'	45°08'	6 Sep 1962	1953	420	5310
4	40°53'	46°33'	8 Sep 1962	1483	550	5207
5	36°30'	46°43'	12 Jul 1960	4360	870	4512
6	32°09'	46°21'	10 Sep 1960	1470	1070	3800
7	28°37'	45°38'	26 Aug 1925	2450	1290	2849

water regime of the Falkland Current prior to its initial mixing with the warm waters of the Brazil Current. This cold water influence is most apparent on the winter cross-section (Fig. 13) in the surface expression of both critical depth and the depth of the DSC axis found on profile 1. Although the actual position of winter profile 1 is 49°48'S, 40°03'W and the profile lies considerably east of the other profiles used to construct the winter sound speed cross-section, it is representative of winter oceanographic conditions at 50°S, 46°30'W. This was determined by comparing the temperature and salinity structures measured by the R/V ATLANTIS II at 52°S, 47°W during August 1980 (published by Georgi, Piola, and Galbraith, 1981). The compared structures were found to be almost identical. During summer (Fig. 12), near-surface warming caused a surface sound speed that is about 42 m/sec higher than that observed during winter. Summer surficial warming also led to shallower sonic layer depths along most of the summer cross-section than those observed along the winter cross-section.

Both the depth of the DSC axis and critical depth increased rapidly to the north along the summer and winter cross-sections. During both seasons, the depth of the DSC axis lay near the depth of the AAIW salinity core. This would be expected since cross-section C lies in the far western South Atlantic over a primary northward flow of AAIW (see Fig. 3). During summer (Fig. 12), the depth of the DSC axis varied from a minimum of 420 m on profile 2 to a maximum of 1100 m on profile 5. For summer profile 2, the AAIW low salinity minimum lay between 337 m and 458 m. For summer profile 5, the AAIW low salinity core lay at 800 m. During winter (Fig. 13), the depth of the DSC axis varied from the surface on profile 1 to approximately 1000 m on profiles 5, 6, and 7. For winter profile 1, the AAIW salinity minimum lay at 53 m, but sank to a maximum depth of 886 m for winter profile 7. Such a rapid and radical change in the depth of the AAIW low salinity core would be expected as the core crossed the Subtropical Convergence zone (between about 35°S and 45°S along 46°30'W). Therefore, the depth of the DSC axis is strongly controlled by the AAIW temperature and salinity structure along cross-section C during both seasons, a similar situation to that observed along cross-sections A and B.

As would be anticipated from the location of cross-section C, the rapid northward increase in critical depth was far more marked during winter (Fig. 13) than during summer (Fig. 12). However, critical depth lay far deeper in the water column during summer than during winter due to the effects of near-surface summer warming along the entire cross-section. Summer critical depth varied from 2340 m on profile 1 to 4190 m on profile 4 and then intersected the bottom at about 35°S (range of about 775 nmi). Winter critical depth varied from the surface on profile 1 to 4080 m on profile 5 and then intersected the bottom at about 33°S (range of about 950 nmi). The upslope decrease in winter critical depth at ranges greater than about 900 nmi is due to near-bottom sound speed changes such as those seen on winter profile 6. These changes most likely are caused by the effects of AABW.

The MIW high salinity core was observable on most of the summer and winter sound speed profiles used to construct Figures 12 and 13. The exception profiles are the last profile for both sections (summer profile 6 and winter profile 7). MIW would not be expected on either profile due to the position of both profiles in shallow water near the Brazil coast (see Fig. 4). On the summer cross-section, the MIW core depth ranged from 2300 m on profile 1. On the winter cross-section, the depth of the MIW core ranged from a depth interval of 1250-2000 m on profile 1 to a depth of 2390 m on profile 2, and had a maximum depth of 2490 m on profile 6. The rapid rise in the depth of the MIW high salinity core between about 45°S and 50°S (i.e., between winter profiles 1 and 2) clearly shows the effect of the Antarctic Convergence and intermixing between AAIW sinking as it flows from the south with

MIW. This process has been described in some detail for the western South Atlantic Ocean by Reid, Nowlin, and Patzert (1977). In general, a mixture of AAIW and MIW or the presence of MIW below the AAIW low salinity core results in higher sound speed structures in the western South Atlantic than those found at similar latitudes east of the Mid-Atlantic Ridge, largely because both MIW and AAIW have primary flows west of the Mid-Atlantic Ridge (see Figs. 3 and 4).

The primary flow of AABW at depths greater than 3500 m also lies west of the Mid-Atlantic Ridge (see Fig. 5). AABW has a near-bottom effect on many of the sound speed profiles used to construct Figures 12 and 13. Generally, AABW causes lesser near-bottom sound speeds throughout the western South Atlantic. This effect is present along sound speed cross-section C during both seasons. The most irregular near-bottom sound speed effects along cross-section C appear on summer sound speed profile 5 (Fig. 12) and winter sound speed profile 16 (Fig. 13). Summer sound speed profile 5 at 32°09'S 46°07'W is perhaps the most irregular profile along the cross-section below a depth of about 3000 m. On this profile, the sound speeds at 3000 m and 3500 m are virtually identical (approximately 1513 m/sec) and apparently are the result of AABW mixing with the bottom of the MIW layer (i.e., intermixing at a depth of about 3000 m). The resulting water mass is extremely dense and is referred to as Lower North Atlantic Deep Water by Reid, Nowlin, and Patzert (1977). A similar, irregular, near-bottom sound speed profile also is found on winter cross-section C (Fig. 13) on sound speed profile 6 (at 32°09'S 46°21'W). In this case, the sound speed varies from 1512.0 m/sec to 1512.9 m/sec between depths of 2990 m and 3490 m. In the opinion of the author, both near-bottom, irregular, sound speed gradients are caused by the mixing of AABW with the bottom of the MIW layer at depths below about 3000 m.

VIII. COMPARISON OF SOUND SPEED AND TEMPERATURE SALINITY STRUCTURE ALONG CROSS-SECTION B

As previously mentioned, cross-section B (see Fig. 11) represents the most important region in the western South Atlantic Ocean in terms of both sound speed and water mass variability. Figure 14 shows a winter sound speed composite along cross-section B. A composite of temperature-salinity (T-S) diagrams along this same cross section is shown in Figure 15. In Figure 15, the T-S diagram for winter profile 14 is not shown. However, this T-S diagram is nearly identical to that for winter profile 12. This would be expected since both profiles 12 and 14 lie within the Equatorial Atlantic (i.e., north of 10°S latitude). A comparison of Figures 14 and 15 shows an extremely large amount of sound speed and T-S variability throughout the water column between 45°S latitude and the Equator along 30°W longitude. This variability is most pronounced at the surface, at the depth of the DSC axis, and at corrected bottom depth. However, variability also occurs throughout the remainder of the water column.

The surface variability in sound speed structure is obviously a function of the surface variability in temperature and salinity. Such variability would be expected along a cross-section that extends from just north of the Antarctic Convergence to the Equator and crosses the cold regime of the Falkland Current, the South Atlantic Subtropical Convergence, the warmer regime of the Brazil Current, and finally ends in the South Equatorial Current (see Fig. 2). A comparison of the sound speed profiles 1 and 12 (Fig. 14) and T-S diagrams 1 and 12 (Fig. 15) gives a good overall view of sound speed and T-S variability between 45°S latitude and the Equator in the western South Atlantic. The surface sound speeds vary from 1482 m/sec (profile 1) to 1536 m/sec (profile 12). Surface temperatures vary from 8.08°C (profile 1) to 25.25°C (profile 12). As shown on Figure 15, near-surface salinity values

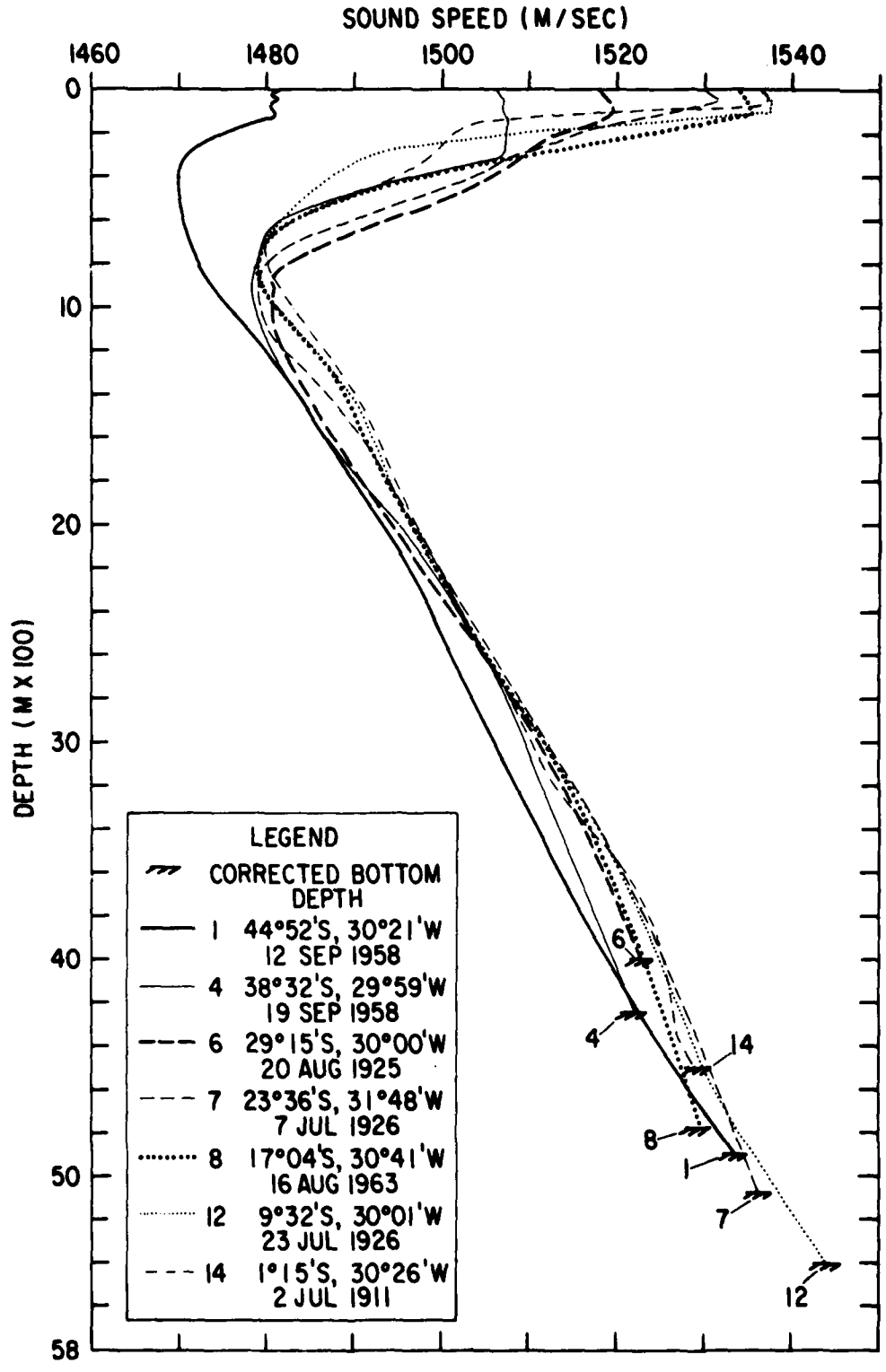

Figure 14. Sound Speed Composite for Winter Cross-Section B

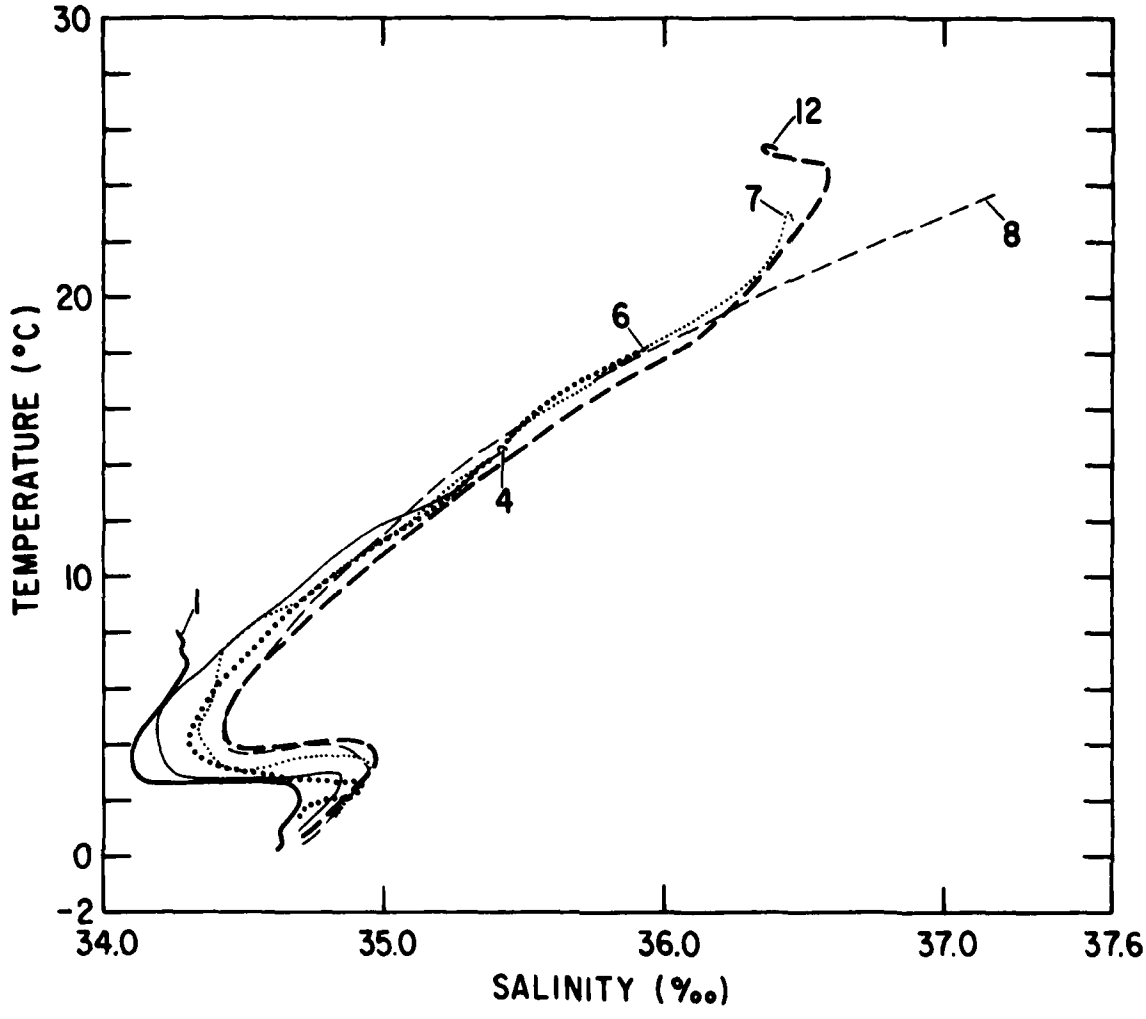

LEGEND		
——	1	44°52'S, 30°21'W, 12 SEP 1958
——	4	38°32'S, 29°59'W, 19 SEP 1958
·····	6	29°15'S, 30°00'W, 20 AUG 1925
	7	23°56'S, 31°48'W, 7 JUL 1926
- - -	8	17°04'S, 30°41'W, 16 AUG 1963
- - -	12	9°32'S, 30°01'W, 23 JUL 1926

NOTE:

T-S DIAGRAM FOR PROFILE 14 (1°50'S, 30°26'W) IS NOT DRAWN.

Figure 15. Temperature-Salinity Composite for Winter Cross-Section B

also show a substantial increase to the north between profiles 1 and 12. However, the highest near-surface salinity shown on Figure 15 (greater than 37.0‰ for profile 8) lies at 17°04'S, 30°41'W, south of the mean position of the South Equatorial Current (see Fig. 2). The location of profile 8 lies closer to the beginning of the Brazil Current. The high salinity in the near-surface layer for profile 8 may be the result of extreme near-surface evaporation during August 1963. However, as shown on Figure 14, this high near-surface salinity for profile 8 does not lead to higher near-surface sound speed values.

As previously mentioned, the depth of the DSC axis roughly corresponds with the depth of the low salinity AAIW core along all of cross-section B. On Figure 15, the AAIW low salinity core is shown by a strong T-S minimum on all five T-S diagrams. For profile 1, the AAIW core lies between 300 m and 700 m at a uniform salinity of 34.11‰. However, temperatures at the AAIW core range between 4.15°C and 2.70°C. This broad, shallow AAIW core at a position south of the South Atlantic Subtropical Convergence (see Fig. 3) leads to a very shallow and low sound speed DSC axis for profile 1 (see Fig. 14). Farther north, the temperature and salinity of the AAIW core increases as the core sinks deeper into the water column. For profile 4, the AAIW core lies at 628 m with a temperature of 5.10°C and a salinity of 34.20‰. For profile 6, the AAIW core has sunk to 880 m with a temperature of 4.19°C and a salinity of 34.32‰ . Salinity at the AAIW core continues to increase as the AAIW core mixes with the remainder of the intermediate water column, including the top of the high salinity MIW layer. This latter mixing has been discussed for the western South Atlantic in detail by Reid, Nowlin, and Patzert (1977). In the opinion of the author, the change in the depth, width, temperature, and salinity of the AAIW core is the primary cause for the variety in the depth and sound speed of the DSC axis found along cross-section B and throughout the remainder of the western South Atlantic Ocean.

Below the depth of the DSC axis and the AAIW low salinity core, sound speed variability along cross-section B is somewhat less until corrected bottom depth is reached. However, variability still exists between various sound speed profiles shown on Figure 14 due to the effects of the MIW high salinity core. As previously mentioned, the MIW high salinity core is found along the extent of cross-section B, but varies in depth between 45°S latitude and the Equator (see Fig. 4). On Figure 15, the MIW core is indicated by a T-S maximum on each of the winter profile T-S diagrams. The temperature and salinity values at the MIW core vary along cross-section B between profiles 1 and 12 by a substantial magnitude. For profile 1, the MIW core is found at 2328 m and 2816 m at temperatures between 2.39°C and 1.76°C and at a uniform salinity of 34.69‰ . For profile 4, the MIW core is found at 2359 m at a temperature of 2.95°C and a salinity of 34.85‰ . Both the temperature and salinity of the MIW core continue to increase to the north along cross-section B until, on profile 12, the core is found at 1980 m at a temperature of 3.31°C and a salinity of 34.97‰ . These changes in the depth, temperature, and salinity at the MIW core are responsible for most of the variability in sound speed structure shown on Figure 14 between the depth of the DSC axis and about 3000 m.

Below about 3000 m depth, the sound speed variability shown on Figure 14 is largely due to the effects of low salinity AABW flowing north from the Antarctic Convergence across the Argentine and Brazil Plains. As previously indicated, the primary northward flow of this near-bottom water mass in the South Atlantic Ocean is to the west of the Mid-Atlantic Ridge (see Fig. 5). The variability in the temperature and salinity values of this water mass along cross-section B is clearly shown

for profiles 1, 6, 7, 8 and 12 in Figure 15. All the six T-S diagrams used to construct Figure 15 have been extended to the corrected bottom. At corrected bottom, the temperatures of the AABW flow vary from 0.21°C for profile 1 to 0.58°C for profile 12. The AABW temperature for profile 14 (not shown on Figure 15) is 0.76°C. The near-bottom salinity of AABW for profile 14 at a shallower corrected bottom depth (3910 m) is 34.72 °/₀₀ , since this profile is located on the southern side of the Rio Grande Plateau (see Fig. 11). However, as indicated on Figure 14, even sound speed profile 6 shows the near-bottom effects of the northward AABW water mass. In fact, the sound speed effects of the near-bottom AABW water mass are apparent on all the sound speed profiles shown on Figure 14. These AABW effects are most apparent on sound speed profiles 1, 4, and 6, all of which lie south of the Rio Grande Plateau. However, AABW effects on near-bottom sound speed structure are also apparent for profiles 7 and 8 that lie over the Brazil Plain on either side of the Victoria Seamounts Rise. The AABW effects on the near bottom sound speed structure for profile 12 are not as pronounced as those for sound speed profiles 7 and 8, but as shown in the T-S diagram for profile 12, AABW is present over the northern Brazil Plain (also see Fig. 5). The near-bottom AABW effects on sound speed profile 14 (located over the Ceara Plain just south of the Romanche Fracture Zone at 1°50'S, 30°26'W) apparently are the effects of intermixing between the bottom of the MIW flow and the top of the AABW flow. Similar intermixing has been observed over the Argentine Plain by Reid, Nowlin, and Patzert (1977) and would be expected south of the Romanche Fracture Zone as the primary northward flow of AABW turns to the west to enter the Atlantic Ocean.

IX. SUMMARY OF SOUND SPEED VARIABILITY IN THE WESTERN SOUTH ATLANTIC

As indicated in the preliminary report on the sound speed structure of the South Atlantic Ocean (Fenner, 1981), sound speed composites are frequently the best indicators of sound speed variability along a baseline. This has been proven true in other oceanic areas such as the North Atlantic Ocean and the North Indian Ocean by the author and others. For the western South Atlantic, three sound speed composites have been constructed to summarize sound speed variability west of the Mid-Atlantic Ridge. These composites are along winter cross-section B (Fig. 14), summer cross-section A (Fig. 16), and winter cross-section A (Fig. 17). All three composites show that significant sound speed variability extends throughout the water column in the western South Atlantic Ocean, but that the variability is most pronounced in the upper water column (i.e., above the depth of the DSC axis in the region of the thermocline).

In the upper water column, the sound speed variability is both temporal and spatial in nature, as would be expected in the region of the thermocline. This variability is best seen by comparing the summer and winter sound speed composites along cross-section A (Figs. 16 and 17). During summer (Fig. 16), all sound speed profiles north of about 38°S latitude (summer profiles 2, 3, 6, 8, 12 14, and 16) have near-surface sound speeds greater than 1520 m/sec due to near-surface warming. Summer sonic layer depths along cross-section A are less than 100 m. Only summer sound speed profile 1 (located at 44°00'S, 51°00'W) has a near-surface sound speed less than 1520 m/sec, and this profile is located south of the South Atlantic Subtropical Convergence in the cold water regime of the Falkland Current. During winter (Fig. 17), only sound speed profiles 6, 7, 9, and 11 have near-surface sound speeds greater than 1520 m/sec. All four of these profiles lie north of 30° latitude within the warm water regime of the Brazil Current and are considerably north of the South Atlantic Subtropical Convergence. Sonic layer depths along cross-section A during winter are generally deeper than those during summer due to the effects of

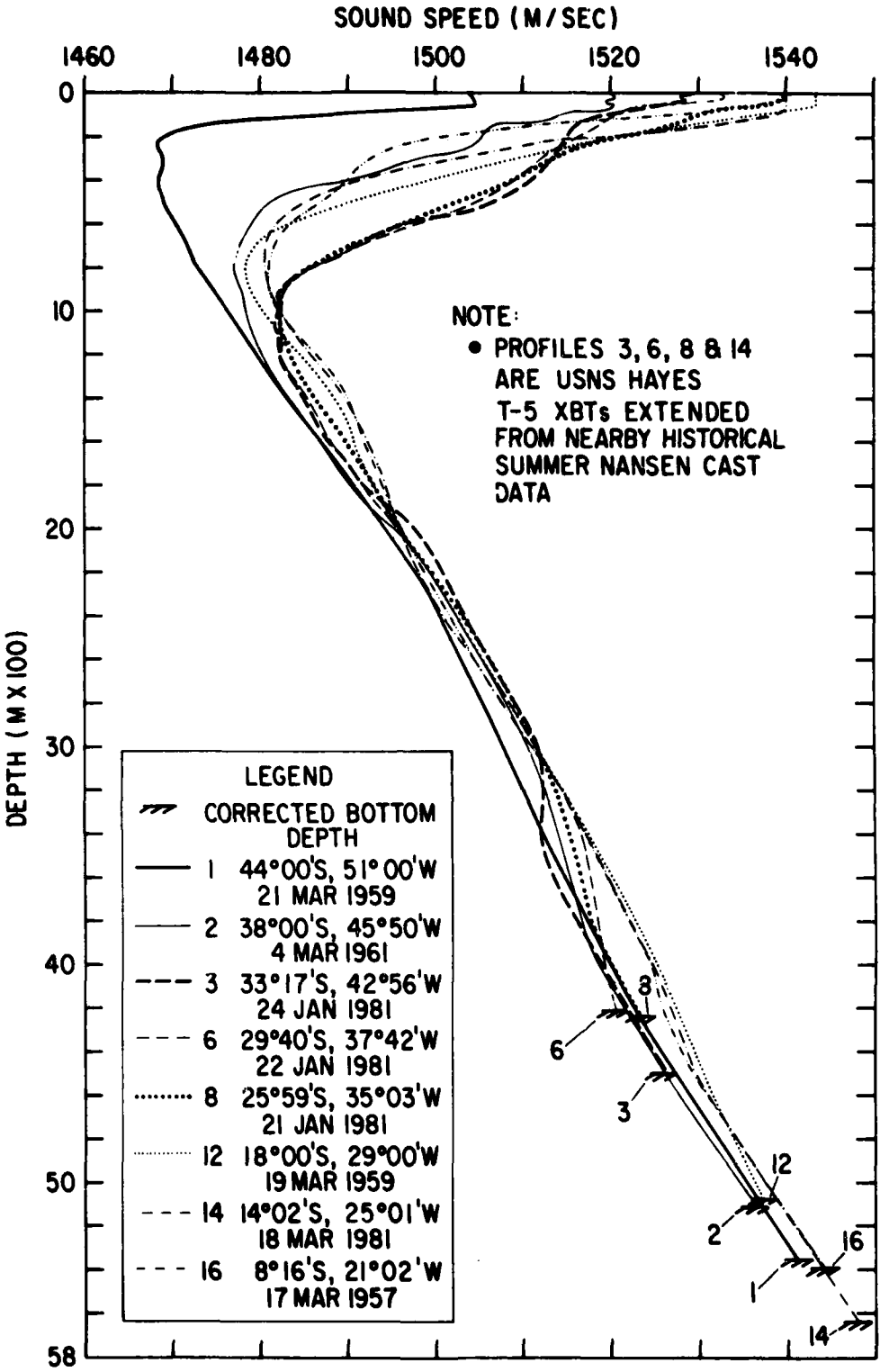

Figure 16. Sound Speed Composite for Summer Cross-Section A

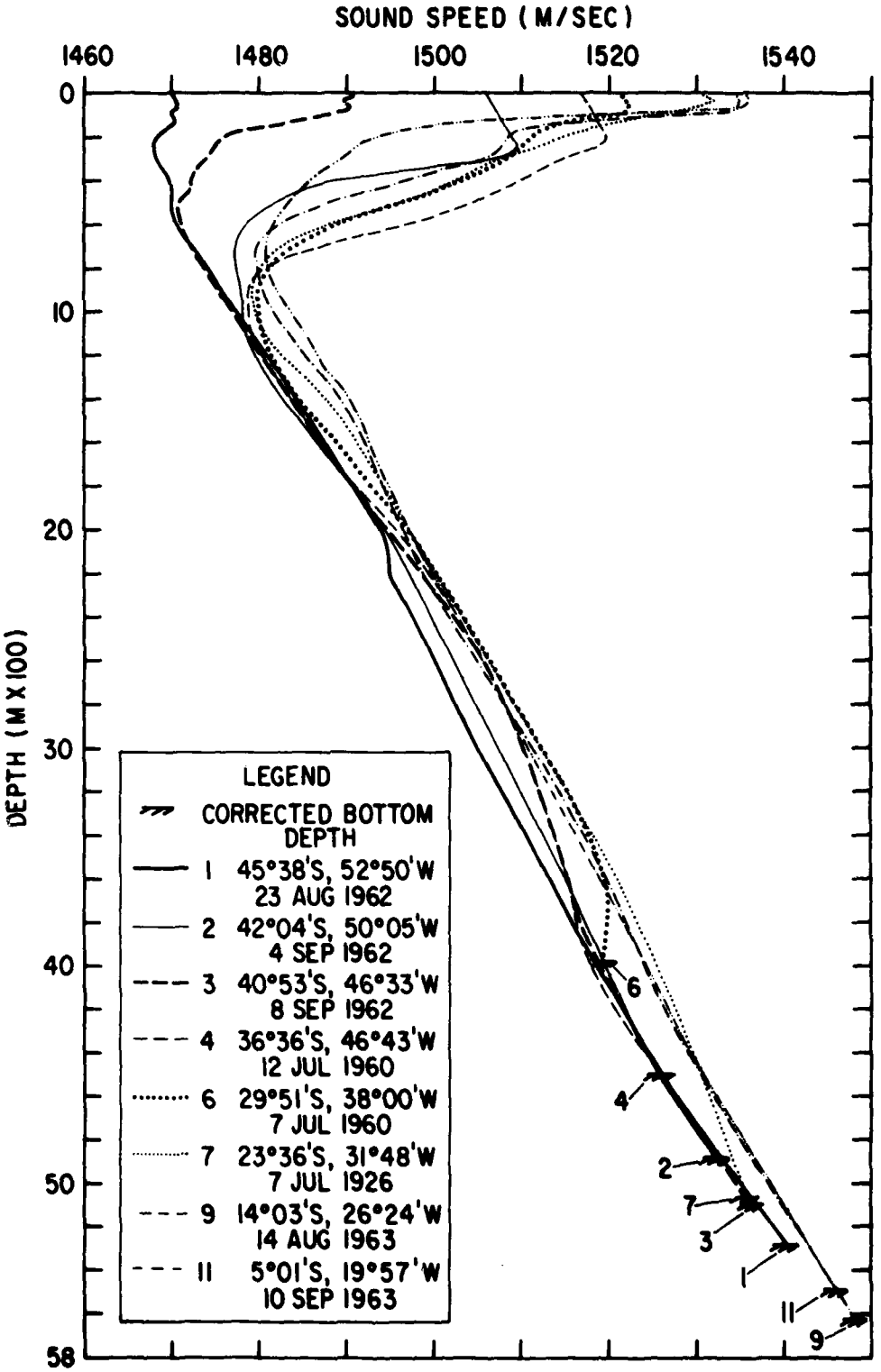

Figure 17. Sound Speed Composite for Winter Cross-Section A

winter near-surface cooling and wind-induced mixing of the near-surface layer. Similar winter effects could be expected throughout much of the western South Atlantic Ocean, particularly in the region south of the Subtropical Convergence.

Along cross-section B (Fig. 14), the winter sound speed composite in the upper mixed layer appears to be somewhat less complex than that along winter cross-section A (Fig. 17). This is probably due to the longitudinal position of cross-section B. Cross-section B lies well to the east of the highly complex oceanographic regime located throughout the upper water column off the South American coast. This upper water column regime is a function of mixing of the colder Falkland Current and the warmer Brazil Current (see Fig. 2), and is particularly complex in the South Atlantic Subtropical Convergence zone. Within the Subtropical Convergence zone, the complex oceanographic structure extends throughout the upper 1000 m of the water column and causes much more variable sound speed structures. Due to the location of the Falkland and Brazil Currents just off the South American coast, sound speed variability would be expected to be greater along cross-section A than along cross-section B during either summer or winter. Even more variability in sound speed structure would be expected in the upper water column along cross-section C that runs south to north along 46°30'W. However, no sound speed composites have been constructed for cross-section C for either summer or winter.

As shown on the cross-section A and cross-section B sound speed composites, the depth of the DSC axis varies from less than 300 m to about 1100 m in the western South Atlantic Ocean. Along both cross-sections, the depth and sound speed of the DSC axis are generally controlled by the northward flow of the AAIW low salinity core. As shown on Figure 3, the predominant flow of this water mass in the South Atlantic Ocean is west of the Mid-Atlantic Ridge at depths less than 1000 m. Changes in the depth, width, and T-S structure of the AAIW core apparently are the primary causes for variation in the depth and sound speed structure of the DSC axis throughout the western South Atlantic Ocean.

Between the depth of the DSC axis and about 3000 m, sound speed variability along cross-sections A and B is primarily due to changes in the depth, width, and T-S structure of the MIW high salinity core. As shown on Figure 4, the predominant southward flow of this water mass in the South Atlantic Ocean also is west of the Mid-Atlantic Ridge for regions north of the South Atlantic Subtropical Convergence zone. When present, the MIW high salinity core causes higher sound speed value than those that occur in the absence of this water mass. The MIW high salinity core also can cause sound speed perturbations at depths between about 1750 m and 2500 m. Perturbations of this nature are found on both the cross-section A and cross-section B sound speed profile composites.

Below a depth of about 3000 m, the near-bottom sound speed variation in the western South Atlantic is far greater than that encountered in the North Atlantic Ocean or the east of the Mid-Atlantic Ridge. This variability is largely due to the effects of low salinity AABW flowing north from the Antarctic Convergence across both the Argentine and Brazil Plains (see Fig. 5). AABW effects in lowering the near-bottom sound speed gradients are most apparent south of the Rio Grande Plateau (30°S latitude) on both the cross-section A and cross-section B sound speed composites. However, AABW effects can occur in the near bottom region as far north as the Equator.

X. REFERENCES

Bowers, J. M. (1971). Fluoride in the South Atlantic and Pacific Oceans. Bedford Institute of Oceanography, Dartmouth, Nova Scotia, Atlantic Oceanography Laboratory Report 1971-4, 7 p.

Broecker, W. W. and H. G. Ostlund (1979). Property Distributions Along the 26.8 Isopycnal in the Atlantic Ocean. J. Geophys. Res., v. 84, n. C3, p. 1145-1154.

Broecker, W. S. and T. Takahasi (1981). Hydrography of the Central Atlantic-- IV. Intermediate Waters of Antarctic Origin. Deep Sea Res., v. 26A, n. 3, p. 177-193.

Buscaglia, J. L. (1971). On the Circulation of the Intermediate Water in the Southwestern Atlantic Ocean. J. Marine Res., v. 29, n. 3, p. 245-255.

Cheney, R. E. and J. G. Marsh (1981). Oceanic Eddy Variability Measured by GEOS 3 Altimeter Crossover Differences. EOS (Trans. Am. Geophys. Union), v. 62, n. 45, p. 743-752.

Defant, A. (1961). Physical Oceanography, v. 1, New York, Pergamon Press, 729 p.

Duedall, I. W. and A. R. Coote (1972). Oxygen Distribution in the South Atlantic. J. Geophys. Res., v. 77, n. 3, p. 496-498.

Fenner, D. F. (1981). Sound Speed Structure of the South Atlantic Ocean (Preliminary). Presented at NAVOCEANO/NORDA South Atlantic Conference, NSTL Station, Miss., August (unpublished).

Feuillet, J. P. (1981). South Atlantic Environmental Acoustic Data Summary. B-K Dynamics, Rockville, Md., December (BKD Tech. Rep TR-3.487), 217 p. (prepared for Surveillance Environmental Acoustic Support Project, Ocean Programs Management Office, NORDA, NSTL Station, MS).

Georgi, D.T., A. F. Amos, K. E. Draganovic, and M. Raymer (1979). STD Observations in the Southwest Atlantic from Cruise 16, Leg 9 of the R/V CONRAD and Cruise 7-75 of the ISLAS ORCADAS. Woods Hole Institution, Woods Hole, Mass. (WHOI Rep. 79-73), August, 121 p.

Georgi, D. T., A. R. Piola, and N. Galbraith (1981). Pressure, Temperature, Salinity and Dissolved-Oxygen Profile Data from R/V ATLANTIS II Cruise 107-Leg X. Woods Hole Oceanographic Institution, Woods Hole, Mass. (WHOI Rep. 81-71), August, 185 p.

Johnson, D. A., S. E. McDowell, L. G. Sullivan, and P. E. Biscayne (1976). Abyssal Hydrography, Nephelometry, Currents, and Benthic Boundary Layer Structure in the Vema Channel. J. Geophys. Res., v. 81, n. 33, p. 5771-5786.

Mackenzie, K. V. (1981). Nine-term Equation for Sound Speed in the Oceans. J. Acoustic. Soc. Am., v. 70, n. 3., p. 807-811.

Matthews, D. J. (1939). Tables of Velocity of Sound in Pure Water and Sea Water for Use in Echo-sounding and Sound-ranging. London, Hydrographic Dept., Admiralty, 56 p. (contained in Handbook of Oceanographic Tables, Naval Occeanogr., Off. SP-68, Washington, D.C., 1966).

Menzel, D. W. and J. H. Ryther (1968). Organic Carbon and Oxygen Minimum in the South Atlantic Ocean. Deep Sea Res., v. 15, n. 3, p. 327-337.

Miller, R. C. (1966). The Sea. New York, Random House, 315 p.

Perry, R. K. (1980). Bathymetry of the South Atlantic Ocean. NRL Acoustics Division, Washington, D.C. (contour manuscript).

Piola, A. R., D. T. Georgi, and M. C. Stalcup (1981). Water Sample and Expendable Bathythermograph (XBT) Data from R/V ATLANTIS II Cruise 107-Leg X. Woods Hole Oceanographic Institution, Woods Hole, Mass. (WHOI Rep. 81-78), 163 p.

Reid, J. L., W. D. Nowlin, Jr., and W. C. Patzert (1977). On the Characteristics and Circulation of the Southwestern Atlantic Ocean. J. Phys. Oceanogr., v. 7, n. 1, p. 62-91.

Sverdrup, H. U., M. W. Johnson and R. H. Fleming (1942). The Oceans, Their Physics, Chemistry, and General Biology. Englewood Cliffs, N. J., Prentice Hall, Inc., 1087 p.

Wilson, W. D. (1960). Equation for Speed of Sound in Seawater. J. Acoustic. Soc. Am., v. 32, n. 10, p. 1357.

Wright, W. R. (1970). Northward Transport of Antarctic Bottom Water in the Western Atlantic Ocean. Deep Sea Res., v. 17, n. 4, p. 367-371.

Wust, G. (1936). Das Bodenwasser und Die Gliederung der Atlantischen Tiefsee (Bottom Water and the Distribution of the Deep Water of the Atlantic). Wissenshaft. Erg. Deutschen Atlantischen Exped. METEOR 1925-1927, B and VI, Teil 1, p. 1-106, Berlin (in German).

Wust, G. (1957). Stoingeschwind Kerten und Strommengein in der Tiefein des Atlantischen Ozeans. Wissenschaft. Eng. Deutschen Atlantischen Exped. METEOR 1925-1927, Band VI. Teil 2, p. 261-420, Berlin (in German).

DISTRIBUTION LIST

Department of the Navy
Asst Deputy Chief of Navy Materials
for Laboratory Management
Rm 1062 Crystal Plaza Bldg 5
Washington DC, 20360 (1)

Department of the Navy
Asst Secretary of the Navy
(Research Engineering & System)
Washington, DC 20350
ATTN: G. A. Cann (1)

Project Manager
ASW Systems Project (PM-4)
Department of the Navy
Washington, DC 20360 (1)

Department of the Navy
Chief of Naval Material
Washington, DC 20360 (1)

Department of the Navy
Chief of Naval Operations
ATTN: OP 987
Washington, DC 20350 (1)

Director
Defense Technology Info Cen
Cameron Station
Alexandria, VA 22314 (1)

Commander
DWTaylor Naval Ship R&D Cen
Bethesda, MD 20084 (1)

Commanding Officer
Fleet Numerical Ocean Cen
Monterey, CA 93940 (1)

Commander
Naval Air Development Center
Warminster, PA 18974 (1)

Commander
Naval Air Systems Command
Headquarters
Washington, DC 20361 (1)

Commanding Officer
Naval Coastal Systems Center
Panama City, FL 32407 (1)

Commander
Naval Electronic Sys Com
Headquarters
Washington, DC 20360 (1)

Commanding Officer
Naval Environmental Prediction
Research Facility
Monterey, CA 93940 (1)

Commander
Naval Ocean Systems Center
San Diego, CA 92152 (1)

Mr. Joe Colborn
Code 304
Naval Ocean Systems Center
San Diego, CA 92152

Commanding Officer
Naval Oceanographic Office (1)

Mr. W. Kaminga
NAVOCEANO Code 7002 (1)

Mr. E. V. Khedouri
NAVOCEANO Code 9000 (1)

Dr. William Hastings
Naval Ocean Systems Center
San Diego, CA 92152 (1)

Mr. J. Kerling
NAVOCEANO Code 7230 (1)

Mr. V. Sprague
NAVOCEANO Code 7210 (1)

Mr. N. DiPiazza
NAVOCEANO Code 7220 (1)

Mr. K. Wilzer
NAVOCEANO Code 7220 (1)

Mr. P. Lorentzen
NAVOCEANO Code 6000 (1)

Ms. Claire Cox
NAVOCEANO Code 7210 (1)

Dr. T. Davis
NAVOCEANO Code 02 (1)

Mr. Charles Ostericher
NAVOCEANO Code 7120 (1)

Mr. John Allen
NAVOCEANO Code 7310 (1)

Mr. Don Atkocius
NAVOCEANO Code 8000 (1)

Mr. Bill Beatty
NAVOCEANO Code 9100 (1)

Commander
Naval Oceanography Command
NSTL Station, MS 39522 (1)

Superintendent
Naval Postgraduate School
Monterey, CA 93940 (1)

Commanding Officer
Naval Research Laboratory
Washington, DC 20375 (2)

Mr. Robert Perry
Naval Research Laboratory
Code 5110
Washington, DC 20375 (1)

Dr. Hank Fleming
Naval Research Laboratory
Code 5110
Washington, DC 20375 (2)

Mr. Bud Adams
Naval Research Laboratory
Washington, DC 20375 (1)

Mr. Eigo Hashimoto
Ocean Data Systems, Inc.
3255 Wing Street
Suite 5500
San Diego, CA 92110 (1)

Dr. J.R.E. Lutjeharms
Physical Oceanography Section
National Research Institute
for Oceanology
P. O. Box 320
7600 Stellenbosch
South Africa (1)

Commander
Naval Sea System Command
Headquarters
Washington, DC 20362 (1)

Commander
Naval Surface Weapons Center
Dahlgren, VA 22448 (1)

Chief of Naval Operations
Department of the Navy
Washington, DC 20350
ATTN: OP-02 (1)
OP-03 (1)
OP-05 (1)
OP-095 (1)
OP-096 (1)
OP-951 (1)
OP-951F (1)
OP-952D (1)

Headquarters
Naval Material Command
Washington, DC 20360
ATTN: MAT-0724 (2)

Project Manager
Antisubmarine Warfare System Proj
Department of the Navy
Washington, DC 20360
ATTN: PM-4 (2)

Director
Strategic System Projects Office
Department of the Navy
Washington, DC 20376
ATTN: PM-1 (1)

Chief of Naval Research
800 North Quincy Street
Arlington, VA 22217
ATTN: Code 100 (1)
Code 102B (1)
Codd 220 (1)
Code 230 (1)
Code 460 (1)
Code 480 (1)

Commander
Naval Electronic Systems Command
Naval Electronic Sys Command Hdqrs
Washington, DC 20360
ATTN: PEM-124 (1)
PME-124T (1)
PME-124/40 (1)
PME-124/60 (1)
ELEX-320 (1)

Commander in Chief
U.S. Atlantic Fleet
Norfolk, VA 23511
ATTN: Code 358 (1)

Commander
Second Fleet
FPO New York, NY 09501 (1)

Commander
Operational Test and Eval. Force
Naval Base
Norfolk, VA 23511
ATTN: Code 42 (1)

Commander
Oceanographic System Atlantic
Box 100
Norfolk, VA 23511
ATTN: Code N34 (1)
Code N36 (1)
Code 012 (1)

Commander
Naval Oceanographic Office
NSTL Station, MS 39529
ATTN: Code 7300 (1)

Dr. F. A. Richards
Scientific Director
Office of Naval Research
Branch Office
223/231 Old Marylebone Road
London NW1 5th, UK (1)

Dr. F. C. Shepard
Marine Biological Laboratory
Woods Hole, MA 02543 (1)

Commander
Naval Ocean Systems Center
San Diego, CA 92152
ATTN: Code 724 (2)
Code 531 (1)
Code 711 (1)

Director
Naval Ocean Surveillance Info Cent
4301 Suitland Road
Washington, DC 20390 (1)

Commanding Officer
Naval Intelligence Support Center
4301 Suitland Road
Washington, DC 20390 (1)

University of Texas
Applied Research Laboratories
P. O. Box 8029
Austin, TX 78712
ATTN: G. E. Ellis (1)
Dr. S. Mitchell (1)

B-K Dynamics
15825 Shady Grove Road
Rockville, MD 20850
ATTN: P. G. Bernard (1)
W. C. Carey (1)

Bell Telephone Labortaories
1 Whippany Road
Whippany, NJ 07981
ATTN: Dr. Frank Benedict (1)

Envo, Inc.
800 Follin Lane
Vienna, VA 22180
ATTN: C. Matheny (1)

Planning Systems, Inc.
7900 Westpark Drive, Suite 600
McLean, VA 22101
ATTN: Dr. R. S. Cavanaugh (1)

Science Applications, Inc.
8400 Westpark Drive
McLean, VA 22101
ATTN: Dr. J. S. Hanna (1)

Tracor, Inc.
1601 Research Blvd.
Rockville, MD 20850
ATTN: J.T. Gottwald (1)

Western Electric Company
P. O. Box 20046
Greensborough, NC 27420
ATTN: G. Manning (1)

Commanding Officer
Naval Eastern Oceanography Center
McAdie Bldg. (U-117)
Naval Air Station
Norfolk, VA 23511 (1)

Commanding Officer
U.S. Naval Oceanography Command Center
Rota, Spain (1)

Commanding Officer
U.S. Naval Oceanography Command Center
Box 31
FPO New York, NY 08540 (1)

Commanding Officer
ONR Branch Office
536 S. Clark Street
Chicago, IL 60605 (1)

Commanding Officer
ONR Branch Office LONDON
Box 39
FPO New York 09510 (1)

Commanding Officer
Naval Underwater Systems Center
Newport, RI 02840 (1)

Commanding Officer
Naval Underwater Systems Center
ATTN: New London Lab
Newport, RI 02840 (1)

Director
New Zealand Oceano Inst
ATTN: Library
P. O. Box 12-346
Wellington N.
New Zealand (1)

Dr. Don Connors
Naval Underwater Systems Center
Code 3635
Newport, RI 02840 (1)

Mr. James DePersis
Defense Technical Information Center
Cameron Station
Alexandria, VA 22134 (1)

Mr. J. Feuillet
B-K Dynamics
15825 Shady Grove Road
Rockville, MD 20850 (1)

Commanding Officer
ONR Eastern/Central Reg Ofs
Bldg 114, Section D
666 Summer St
Boston, MA 02210 (1)

Commanding Officer
ONR Western Regional Ofs
1030 E. Green Street
Pasadena, CA 91106 (1)

President
Texas A & M
ATTN: Dept of Ocean Working Collection
College Station, TX 77843 (1)

Director
University of California
Scripps Institute of Oceanogrpahy
P. O. Box 6049
San Diego, CA 92106 (1)

Dr. P. R. Tatro
Science Applications, Inc.
1710 Goodridge Dr.
McLean, VA 22102 (1)

Mr. R. T. Williams
Physical and Chemical Oceanogrpahic Data Facility
Scripps Institute of Oceanography
University of California, San Diego
La Jolla, CA 92093 (1)

Dr. George Anderson
Physical and Chemical Ocenaographic Data Facility
Scripps Institute of Oceanography
University of California, San Diego
La Jolla, CA 92093 (1)

Director
University of Washington
Department of Ocenaography
Seattle, WA 98195 (2)

Dr. Raplph R. Goodman
SACLANT ASW Research Center
La Spezia, ITALY (2)

Dr. V. C. Anderson
Scripps Institute of Oceanography
Marine Physical Laboratory
San Diego, CA 92152 (1)

Director
Woods Hole Ocenaographic Institute
Woods Hole, MA 02543 (1)

Dr. A. R. Piola
Woods Hole Ocenaographic Institute
Woods Hole, MA 02543 (1)

Dr. D. T. Georgi
Woods Hole Oceanographic Institute
Woods Hole, MA 02543 (1)

Dr. John Bruce
Woods Hole Oceanographic Institute
Woods Hole, MA 02543 (1)

Dr. R. L. Fisher
Scripps Institute of Oceanography
University of California, San Diego
La Jolla, CA 92093 (1)

Dr. Arnold L. Gordon
Lamont-Doherty Geological Observatory
Palisades, NY 10964 (1)

Dr. K. V. Mackenzie
P. O. Box 80715, Midway Station
San Diego, CA 92138 (1)

NORDA CODE

100	Commanding Officer	(1)
101	Executive Officer	(1)
102	Procurement Officer	(1)
103	Security Manager	(1)
104	Public Affairs Officer	(1)
106	Deputy EEP Officer	(1)
110	Technical Director	(1)
111	Asst to Technical Director	(1)
115	Environmental Requirements and Program Analysis Group	(1)
120	Administration Office	(1)
121	Management Services	(1)
124	Facilities Services	(1)
125	Technical Information	(1)
130	NORDA Liaison Office	(2)
140	Civilian Personnel Division	(2)
150	Patent Counsel	(1)
160	Financial Management Division	(2)
180	Ship Management Office	(1)
300/ 301/ 310	Ocean Science & Technology Lab (OSTL)	(2)
320	Numerical Modeling	(3)
330	Oceanography	(1)
340	Ocean Acoustics	(3)
350	Ocean Technology	(1)
360	Sea Floor	(1)
370	Mapping, Charting & Geodesy	(1)
500/ 510	Ocean Programs Management Office	(2)
520	Surveillance Environmental Acoustic Support (SEAS)	(4)
530	Tactical ASW Environmental Acoustic Support (TAEAS)	(1)
540	Ocean Measurements	(1)
550	Mapping, Charting & Geodesy Program	(1)
ONRDET Director, ONR Science & Technology Detachment, Bay St. Louis, MS		(2)

UNCLASSIFIED

SECURITY CLASSIFICATION OF THIS PAGE (When Data Entered)

REPORT DOCUMENTATION PAGE		READ INSTRUCTIONS BEFORE COMPLETING FORM
1. REPORT NUMBER NORDA Technical Note 107	2. GOVT ACCESSION NO. AD-A118765	3. RECIPIENT'S CATALOG NUMBER
4. TITLE (and Subtitle) Sound Speed Structure of the Western South Atlantic Ocean		5. TYPE OF REPORT & PERIOD COVERED Final 6. PERFORMING ORG. REPORT NUMBER
7. AUTHOR(s) Don F. Fenner		8. CONTRACT OR GRANT NUMBER(s)
9. PERFORMING ORGANIZATION NAME AND ADDRESS Naval Ocean Research & Development Activity Ocean Programs Management Office, Code 500 NSTL Station, Mississippi 39529		10. PROGRAM ELEMENT, PROJECT, TASK AREA & WORK UNIT NUMBERS
11. CONTROLLING OFFICE NAME AND ADDRESS Same		12. REPORT DATE July 1982 13. NUMBER OF PAGES 43
14. MONITORING AGENCY NAME & ADDRESS(if different from Controlling Office)		15. SECURITY CLASS. (of this report) UNCLASSIFIED 15a. DECLASSIFICATION/DOWNGRADING SCHEDULE

16. DISTRIBUTION STATEMENT (of this Report)

Unlimited

17. DISTRIBUTION STATEMENT (of the abstract entered in Block 20, if different from Report)

18. SUPPLEMENTARY NOTES

19. KEY WORDS (Continue on reverse side if necessary and identify by block number)

Sound speed, Western South Atlantic Ocean, Temperature-Salinity, South Atlantic Subtropical Convergence, Antarctic Convergence, Sonic Layer Depth, Deep Sound Channel Axis, Critical Depth, Acoustic Propagation, Antarctic Intermediate Water, Mediterranean Intermediate Water, Antarctic Bottom Water, South Equatorial Current, Brazil Current, Falkland Current.

20. ABSTRACT (Continue on reverse side if necessary and identify by block number)

The sound speed structure of the western South Atlantic Ocean is far more variable than that found in the North Atlantic or North Indian Oceans, largely due to hemispheric position and a wide variety of surface, near-surface, intermediate depth, and near-bottom water masses. In the South Atlantic, summer is defined as January-March and winter as July-September. The wide variety of temperature and salinity variability throughout the western South Atlantic leads to entirely differently shaped sound speed profiles and entirely different

DD FORM 1 JAN 73 1473 EDITION OF 1 NOV 65 IS OBSOLETE
S/N 0102-LF-014-6601

UNCLASSIFIED

SECURITY CLASSIFICATION OF THIS PAGE (When Data Entered)

20. ABSTRACT (Continued)

values of the depth of the deep sound channel axis and critical depth. These differences undoubtedly have significant effects on acoustic propagation. This report examines western South Atlantic sound speed variability along three cross-sections for both summer and winter, relates variability in sound speed structures to surface currents, the Antarctic Intermediate Water, Mediterranean Intermediate Water, and Antarctic Bottom Water core flows west of the Mid-Atlantic Ridge, and defines the number of observations deeper than the depth of the deep sound channel axis during both summer and winter for the entire South Atlantic Ocean between the Equator and 45°S latitude.

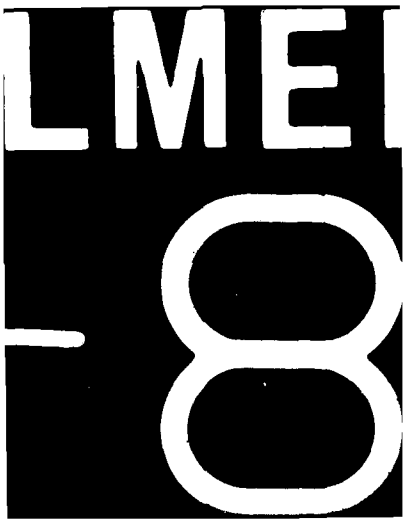
LME
8